IEEE Access
Multidisciplinary | Rapid Review | Open Access Journal

Received 8 April 2024, accepted 20 May 2024, date of publication 23 May 2024, date of current version 3 June 2024.

Digital Object Identifier 10.1109/ACCESS.2024.3404497

RESEARCH ARTICLE

Advanced Control Strategies for Photovoltaic Power Quality and Maximum Power Point Tracking Optimization

MPHO SAM NKAMBULE, ALI NABIL HASAN, AND THOKOZANI SHONGWE, (Senior Member, IEEE)
Department of Electrical and Electronic Engineering Science, University of Johannesburg, Johannesburg 2006, South Africa
Corresponding author: Mpho Sam Nkambule (nkambule833@gmail.com)

This work was supported in part by the University of Johannesburg.

ABSTRACT This paper introduces an innovative Expectation-Conjugate-Gradient (ECG) approach designed for the management of the interfacing inverter in a grid-connected fixed tilt bifacial Photovoltaic (PV) system. The focus of this algorithm is to address current harmonics issues and elevate power quality. Additionally, the proposed control strategy integrates with an Enhanced Dual second-order generalized integrator phase-locked loop (EDSOGI-PLL), enhanced with a Savitzky-Golay Filter (SGF) to achieve grid synchronization, mitigate voltage harmonics, and estimate symmetrical components during unbalanced grid conditions. The state-of-art Double deep Q-network (DDQN) maximum power point tracking algorithm is introduced, integrating centralized start-up condition computation to stabilize voltage levels at the shared DC-link bus terminal. Key benefits include reduced harmonics, enhanced stability, adaptive control, and minimal computational load. Simulation confirms compliance with IEEE 519 Standards, THD $< 3\%$, PF ≈ 1, and reveal a significant reduction in CO2 emissions.

INDEX TERMS Expectation-conjugate-gradient, double deep q-network, bifacial photovoltaic system, power quality, maximum power point tracking, total harmonic distortion.

I. INTRODUCTION

The usage of renewable energy sources such as solar photovoltaic (PV) has gained increased attention in recent years due to the diminution of fossil fuel, swift industrialization, freely available, low maintenance costs, and technological development [1]. In particular, bifacial PV (bPV) modules technology are notably gaining attention due to the potential of obtaining additional energy from the rear-side solar insolation. Furthermore, the power gain of bPV modules can be 25% higher than of a monofacial PV (mPV) modules under optimized installation configuration [2]. Unavoidably, the solar PV system has been connected into utility grid distribution utilizing numerous power processing units. However, the PV system has a few disadvantages such as low voltage generation, and difficulty in tracking global maximum power point (GMPP) due to complex weather conditions. The partial shading conditions (PSC) is generally caused by passing clouds, dust, shades from trees, etc., as a result, the PV panel efficiency is compromised. Another major challenge is the low power quality due to the usage of power electronics converters and nonlinear loads [3]. This causes harmonic distortion in the current injected into the grid and consequently, grievously influences the system's power quality. The harmonics can result in grid voltage fluctuations, annoyance trips, voltage flickering, overheating of electrical equipment, unintentional disconnections of the PV system, electrical device failure due to excessive voltage distortion, shortening of the life of the electrical equipment, and ultimately lower system power factor leading to high monthly utility costs. These elements serve as the impetus for the researchers' decision to focus their study on harmonic compensation and maximum power point tracking (MPPT) controllers for power quality improvement.

The associate editor coordinating the review of this manuscript and approving it for publication was Nagesh Prabhu.

To improve the PV module efficiency under rapidly changing weather conditions, researchers proposed optimization algorithms for GMPP tracking under PSC. The Ant colony bee optimization [4], Atom search optimization (ASO) [5], Harmony search optimization [HSO], are proposed as these techniques can track GMPP. However, all these techniques suffer from large oscillations and convergence around GMPP. In [6] and [7], Harris Hawk Optimization (HHO), Golden eagle optimization (GEO), and Modified Gray Wolf Optimization Algorithm [8], have been proposed for fast GMPP tracking. The algorithms demonstrated fewer oscillations and reliable convergence. These systems, however, suffer from needless GMPP searches and have power losses because the restart condition is not taken into account. The reinitializing conditions present the biggest problems for global search algorithms. The operation of PV systems depends on avoiding pointless searching and offering an assertive GMPP restarting condition.

To improve the output power of PV modules in PSC, various optimization algorithms have been proposed for tracking the GMPP amidst rapidly changing environmental factors. Researchers have introduced algorithms like Particle Swarm Optimization (PSO) [9], Enhanced Dandelion Optimizer [10], Bat algorithm [11], and Neuro Fuzzy inference system [12] due to their effectiveness in GMPP tracking. However, these algorithms often exhibit significant oscillations and struggle with convergence issues around GMPP. In an attempt to address these challenges, an Improved (Cuckoo Search) CS MPPT algorithm was proposed in [13], utilizing three search agents for power optimization through the combination of Levy flight and the distance between search agents. Additionally, a multi-universe optimization algorithm method was introduced in [14] to mitigate high oscillations and reduce convergence time. Nevertheless, these approaches led to increased controller complexity, potentially resulting in higher installation and commissioning costs.

Another avenue explored in [15] involved hybrid algorithms such as CS combined with Fuzzy Logic Controller (FLC), Genetic algorithm (GA) and Gated recurrent unit (GRU) [16], aiming for swift GMPP tracking by leveraging the advantages of both algorithms. Although these hybrid methods demonstrated fewer oscillations and reliable convergence, they faced drawbacks such as unnecessary GMPP search and subsequent power losses due to the lack of consideration for restarting conditions. One of the main challenges associated with global search techniques lies in addressing restarting conditions. It is crucial to avoid unnecessary searches and establish a robust GMPP restarting condition for the efficient operation of PV systems.

To maintain the power quality within acceptable standards in the grid, inverter control schemes play a vital role in a grid-connected PV system. The authors in [17], [18], [19], and [20], proposed Newton-Raphson (NR), Improved linear sinusoidal tracer (ILST), Genetic algorithm (GA) and Bee algorithm (BA) to minimize harmonics and to control the grid injected reactive power. However, these control strategies have some limitations such as inadequate tracking of steady-state response, low weight convergence rate, high complexity, and computational burden. Furthermore, these algorithms are not effective under nonlinear loads or transient state.

In a grid-tied PV system, the effective control of inverters is pivotal to ensure the quality of power fed into the grid. A study conducted by Babu et al. [18] introduced a Proportional-Integral (PI) current controller for the grid-interfacing inverter. This controller aimed to make the output current mimic a predetermined reference current, derived from the required power transfer to the grid. However, a limitation of this controller surfaced in its inefficacy under nonlinear loads and unbalanced conditions.

Addressing this challenge, Authors in [21] proposed the use of Quasi-Recurrent Neural Network (QRNN) to minimize harmonics and regulate the reactive power injected into the grid. Despite its potential, this algorithm faced difficulties in determining the appropriate learning parameters. Additionally, recent adaptive control techniques like Recursive Least Square (RLS) [22], Improved Linear Sinusoidal Tracer (ILST) [23], Variable Step-Size Least Mean Square (VSS-LMS) [24], and Least Mean Fourth (LMF) [25] have been introduced. However, these techniques are not without limitations, including inadequate tracking of steady-state response, slow convergence rates, high complexity, and computational burden.

To overcome the aforementioned challenges, alternative control techniques have been proposed. The Second-Order Generalized Integrator (SOGI), Adaptive Differentiation Frequency (ADF) [26], and Multiple Complex Coefficient Filter (MCCF) based Phase-Locked Loop (PLL) [27] have been suggested for rejecting current and voltage harmonics. These approaches offer potential solutions without the drawbacks associated with the previously mentioned control strategies.

Despite their impressive performance, the aforementioned approaches fall short when dealing with nonlinear loads. As a result, there is a demand for a novel inverter control strategy that not only adapts and organizes itself but also outperforms existing methods in attenuating harmonics during both steady-state and transient states.

This study introduces the DDQN MPPT technique aimed at stabilizing the DC voltage level at the common DC bus under PSC conditions. Existing approaches often neglect the need to restart the GMPP, leading to significant issues with global search algorithms. This work emphasizes the importance of providing an assertive GMPP restarting condition to avoid futile searches in PV systems. Additionally, a self-adapting Expectation-Conjugate-Gradient (ECG) technique is proposed to manage the interface inverter of grid-tied PV systems, effectively reducing current harmonics, and enhancing power quality. Moreover, an improved ECG based on HBM is presented for grid synchronization, voltage harmonics attenuation, and symmetrical component estimation in unbalanced grid scenarios. Results obtained from

MATLAB Simulink simulations underscore the superiority of the newly proposed grid-integrated PV system. Following is a summary of how the innovation of this research adds to the suggested work:

- A proposed grid tied bifacial PV system with a fixed tilt configuration at Johannesburg location using PVSyst software and environmental analysis.
- A novel DDQN MPPT algorithm with a centralized start-up condition computation is introduced to enhance PV system power tracking under PSC, ensuring stable DC voltage and minimizing voltage fluctuations during transient states. The DDQN is compared with existing GEO MPPT algorithm.
- An ECG technique is proposed to reduce harmonics. It incorporates an inverter management strategy for calculating three-phase reference voltages, enabling optimized PWM signal generation for improved grid-tied inverter performance and enhanced power quality in grid-connected PV systems.
- The novel ECG integrated with EDSOGI-PLL (modified with SGF) is proposed for grid synchronization, voltage harmonics attenuation, and symmetrical components estimation under unbalanced grid conditions, steady-state, and transient states.
- Furthermore, the second stage of harmonic mitigation is proposed using the Sequential Cascaded Harmonic Blocking Module (HBM) with the aim of precisely mitigating the emergence of low-order harmonics.
- To assess the proposed system's power quality, the proposed ECG inverter control technique is contrasted with ASO & QRNN and subjected to a fast Fourier transform (FFT) analysis.

The paper's structure is as follows: Section II explains the proposed system, Section III introduces MPPT and inverter control algorithms, Section IV presents the system setup, and Section V demonstrates results and discussions. Finally, Section VI concludes the paper, summarizing key findings and contributions.

II. SYSTEM DESCRIPTION

A. CRITICAL ANALYSIS OF BIFACIAL PV MODULES ON A FIXED TILT CONFIGURATION

A critical analysis of bifacial PV panels on a fixed tilt configuration using a SWOT analysis framework provides a comprehensive evaluation of its strengths, weaknesses, opportunities, and threats as shown in Table 1.

TABLE 1. A comparison between the proposed EDSOGI-PLL and the standard DSOGI-PLL.

Parameters	Standard DSOGI-PLL	Proposed EDSOGI-PLL
Settling time	35ms	15ms
Frequency overshoot	35%	1%
Phase overshoot	8°	9°

Bifacial photovoltaic (PV) panels on a fixed tilt configuration offer several strengths, including enhanced energy generation from both front and back surfaces, higher efficiency through utilization of reflected sunlight, design flexibility, and reduced land requirements. However, limitations such as limited sunlight capture optimization, sensitivity to ground albedo, and higher upfront cost compared to mPV panels should be considered. Opportunities exist in technological advancements, increased adoption, and emerging applications. Threats include regulatory uncertainties, competition from other PV technologies, and potential degradation and durability issues. Overall, bifacial panels on a fixed tilt configuration demonstrate promise but require careful assessment and optimization to ensure their successful implementation.

Strengths

- Enhanced Energy Generation: Bifacial panels generate electricity from both sides, increasing energy production.
- Higher Efficiency: They utilize reflected sunlight, boosting overall efficiency and energy yield.
- Design Flexibility: Bifacial panels can be easily integrated into fixed tilt configurations, requiring less maintenance than tracking systems.
- Reduced Land Requirements: Their higher power densities result in reduced land requirements for PV installations.

Weakness

- Limited Sunlight Capture: Fixed tilt configurations may not optimize exposure to varying solar angles, leading to suboptimal performance and reduced energy generation potential.
- Albedo Sensitivity: Bifacial panels' rear-side power generation relies on ground reflectivity, which can be limited if the ground has low reflectivity.
- Higher Cost: Bifacial panels generally have a higher upfront cost than mPV panels, potentially impacting the overall economics and return on investment of a PV system using fixed tilt bifacial panels.

Opportunities

- Technological Advancements: Ongoing research is improving the efficiency and cost-effectiveness of bifacial panels, enhancing their performance in fixed tilt setups.
- Increased Adoption: Growing interest in renewable energy and declining PV technology costs create opportunities for wider adoption of bifacial panels in fixed tilt configurations.
- Emerging Applications: Fixed tilt bifacial panels are well-suited for solar farms, commercial rooftops, and ground-mounted systems in locations with favorable ground reflectivity.

Threats

- Regulatory and Policy Uncertainties: Government policies and regulations regarding solar energy can impact the economic viability and market dynamics for fixed tilt bifacial panels.

- Competition from Other PV Technologies: Other PV technologies and alternative energy generation methods may present competitive challenges to the adoption of bifacial panels in fixed tilt setups.
- Potential Degradation and Durability Issues: Being a relatively new technology, the long-term performance, degradation, and durability of bifacial panels in fixed tilt configurations need careful assessment to ensure reliability and longevity.

B. PARTIAL SHADING CONDITIONS EFFECT

Partial Shading Conditions (PSC) pose a substantial threat to the operational efficacy of solar farms, significantly impacting the performance of PV systems. The introduction of shading onto PV modules initiates what is known as the ''partial shading effect,'' inducing disparities in the current-voltage characteristics between shaded and unshaded segments. This discrepancy translates into a tangible reduction in overall power output, potentially giving rise to hotspots and contributing to the degradation of modules over time. The intricacies intensify when confronted with the challenge of MPP tracking, exacerbating the overall reduction in energy production.

Effectively addressing PSC necessitates the deployment of advanced power electronics, prominently exemplified by MPPT. This technology plays a pivotal role in optimizing module performance by dynamically adjusting the operating point to the true MPP. Accompanying MPPT, the integration of shading analysis tools becomes imperative, facilitating a nuanced understanding of the shading patterns and their impact on the PV system. Moreover, layout optimization strategies assume critical importance in mitigating the adverse effects of partial shading, aiming to strategically position panels to minimize shading occurrences and enhance overall energy yield.

In the pursuit of maximizing energy yield and efficiency in solar farms grappling with PSC, meticulous system design and the implementation of effective mitigation strategies are paramount. This involves the judicious incorporation of advanced power electronics, particularly MPPT, to optimize the performance of individual modules while intelligently bypassing shaded areas. Comprehensive analysis, augmented by sophisticated shading mitigation algorithms, plays a crucial role in overcoming the multifaceted challenges posed by PSC, ensuring the sustained and optimal functionality of the solar system.

It is essential to acknowledge the disadvantages associated with PSC, as they cast a shadow on the overall performance of PV systems. The reduction in power output due to shading not only limits the energy production capacity but can also lead to thermal imbalances, creating hotspots and accelerating module degradation. Furthermore, the complexity introduced by PSC makes the tracking of GMPP challenging, contributing to an overall decline in the efficiency of the PV system. These drawbacks underscore the critical need for innovative solutions and advanced technologies to mitigate the adverse effects of partial shading conditions and bolster the resilience of solar farms.

C. HARMONICS EFFECT

Undesirable electrical frequencies, commonly referred to as harmonics, represent a significant challenge in grid-tied PV systems. These harmonics, characterized by deviations from the ideal sinusoidal waveform, primarily emanate from power electronic devices such as inverters and DC-DC converters. Interactions with other nonlinear loads connected to the grid further contribute to their generation. The deleterious consequences of harmonics encompass voltage and current distortions, diminished system efficiency, and potential repercussions on the performance and lifespan of sensitive loads and equipment. Additionally, harmonics can interfere with protective devices and control systems, inducing grid instability.

To effectively tackle the challenges posed by harmonics, the implementation of robust mitigation strategies is imperative. Leveraging advanced power electronic devices equipped with harmonic filtering capabilities proves instrumental in curtailing harmonic emissions at their source. Both active and passive filtering techniques, exemplified by active power filters, harmonic compensators, machine learning-driven control strategies, and dedicated harmonic filters, play crucial roles in ameliorating harmonics and enhancing power quality. Adherence to grid codes and industry standards is paramount to ensuring that harmonic levels remain within permissible limits, thereby upholding the stability of the utility grid.

Expanding on the disadvantages associated with harmonics in grid-tied PV systems, it is crucial to recognize their potential to induce further complexities. High levels of harmonics not only lead to increased voltage and current distortions but can also instigate equipment overheating, exacerbating the risk of premature equipment failure. Moreover, harmonics can compromise the accuracy and reliability of power meters, resulting in erroneous measurements and billing discrepancies. The presence of harmonics may also necessitate the installation of oversized equipment to accommodate the distorted waveforms, leading to additional costs and reduced overall system efficiency.

Identifying the root causes of harmonics in grid-tied PV systems is paramount in formulating effective mitigation strategies. In addition to power electronic devices and nonlinear loads, intermittent cloud cover causing fluctuations in solar irradiance and load variations contribute to harmonic disturbances. These external factors necessitate a comprehensive approach to harmonics management, incorporating real-time monitoring and control systems for swift detection and diagnosis. Timely mitigation actions, informed by accurate monitoring, are essential to optimize the performance and efficiency of grid-tied PV systems while ensuring compliance with stringent quality standards and grid stability.

III. PROPOSED CONTROL ALGORITHMS

A. DOUBLE DEEP Q-NETWORK

An improvement on the Deep Q-Network (DQN) method used in reinforcement learning is the Double Deep Q-Network (DDQN). In order to solve Markov Decision Processes (MDPs), the DQN technique blends deep neural networks with Q-learning. [18]. DDQN improves upon the original DQN algorithm by addressing its tendency to overestimate action values. The main principle of DDQN is to separate the decision-making process for actions from the assessment of those actions during the learning process. Two distinct neural networks—the target network and the online network—are introduced to achieve this decoupling. The target network is utilized to calculate the estimated Q-values associated with these activities, while the online network is in charge of choosing the actions.

The DDQN approach calculates the Q-values using a deep neural network as a function approximator. This network generates a Q-value for each potential action based on the input of the environment's state. The agent interacts with the environment while being trained, perceiving states, acting, and being rewarded. These experiences are stored in a replay buffer, which acts as a memory to store and randomly sample from past experiences. To address the overestimation bias, DDQN introduces a separate target network. The online network is duplicated in the target network, but the weights are frozen. It receives updates less frequently than the online network. The Q-value targets for the online network's training are produced using the target network.

As opposed to the original DQN, which estimated the ideal action by utilizing the maximum Q-value from the target network, DDQN selects the action by using the online network. The target network is then used to analyze this activity in order to determine the matching Q-value. DDQN seeks to lessen the overestimation bias seen in DQN by separating the selection and evaluation processes. The DDQN training procedure comprises reducing the mean squared error between the target Q-value acquired from the target network and the Q-value predicted by the online network. The reward acquired from the environment and the discounted maximum Q-value of the subsequent state, as determined by the target network, are added to create the Q-value target. Target network update is a method that DDQN uses to further stabilize the learning process. The weights of the target network are updated periodically, usually with a soft update, where a fraction of the online network's weights is transferred to the target network. This update strategy helps to make the target network's estimates more stable and less prone to fluctuations. DDQN visualization can be demonstrated using Fig.1.

DDQN can be represented mathematically as follows:

First, we select an action for the next state (s') using the online Q-Network:

$$a' = argmax(Q\_online(s', a)) \tag{1}$$

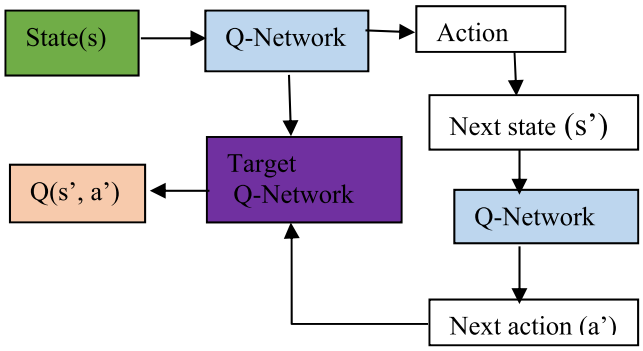

FIGURE 1. DDQN block diagram.

The target Q-value is then determined for the following state (s') and the chosen action (a') using the target Q-Network:

$$Q\_targ(s, a) = r + \gamma * Q\_targ(s', argmax(Q\_online(s', a))) \tag{2}$$

where:

- "$Q\_targ(s, a)$: Target Q-value for state s and action a".
- "r : Immediate reward received after taking action$a$ in state s."
- "γ: Discount factor, a value between 0 and 1, which discounts the importance of future rewards."

Changing from $Q(s)$ to $Q(s, a)$ in DDQN enables a more precise evaluation of the quality of actions in different states, enhancing decision-making accuracy. This transition allows the algorithm to better capture the nuanced relationships between states and actions, leading to improved approximation of expected future rewards for each action taken.

"Update the online Q-Network using the Mean Squared Error (MSE) loss between the predicted Q-value and the target Q-value":

$$Loss = MSE(Q\_online(s, a), Q\_target(s, a)) \tag{3}$$

In order to update the parameters of the online Q-Network, perform gradient descent on the loss. To stabilize the learning process, periodically update the target Q-Network by replicating the weights of the online Q-Network.

The DDQN algorithm represents a significant advancement over its predecessor, DQN, by addressing the issue of overestimation bias. Through the careful separation of action selection and evaluation processes using two distinct neural networks, coupled with the incorporation of experience replay and a soft target network update strategy, DDQN achieves enhanced stability, convergence, and sample efficiency in solving complex reinforcement learning problems. The mathematical formulation further solidifies the algorithm's theoretical underpinnings, providing a comprehensive understanding of its functioning in Markov Decision Processes.

B. CENTRALIZED START-UP CONDITION COMPUTATION

The process of unnecessary exploration can be intricate and may lead to power inefficiencies when PV system is already functioning at its GMPP. It is crucial and rational for the MPPT controller to initiate a new GMPP search only when the PV system is operating at the local Maximum Power Point MPP. The start-up condition can be triggered by monitoring power, insolation level, and changes in cell temperature. However, relying solely on power, irradiance, and temperature change as restart conditions may be misleading during morning and afternoon intervals, necessitating significant investment in meteorological towers to address this challenge.

An alternative approach involves using a time-delay method for GMPP search at predefined intervals. Unfortunately, this method lacks the ability to identify PSC, leading to unnecessary restart conditions at specific time windows. This poses a significant challenge that needs to be resolved to prevent unnecessary power losses and oscillations.

To address this issue, this paper proposes a novel algorithm for a start-up condition that can distinctly identify underperforming MPPT arrays and trigger restart conditions for these specific arrays. The proposed control topology is capable of assessing and analyzing the performance of individual arrays. Typically, a PV system consists of multiple inverters, each comprising one or more arrays. Each array is equipped with a dedicated MPPT controller. The proposed centralized topology can aggregate the power produced by each array. In the event of shading in a particular PV array, the controller activates a restart condition for that shaded array upon receiving a trigger signal after detecting the shade. Centralized topology employs data analysis to identify underperforming PV arrays. The Average Absolute Deviation (AAD) is utilized as a robust statistical tool for outlier detection, involving a three-step process to compute the average dataset from a central point.

1) SCREENING THE DATASET

The reset condition topology starts the filtering process for each sample, i, by filtering the measured values N from each array. AAD serves as the basis for the filter process, which considers a time span of T prior measurements, maps those measurements, and returns the average value for that time.

Measured power P_i^n at i^{th} sample, the average for each array is computed utilizing equation (4).

$$A_i^n = Average(P_i^n, P_{i-1}^n, \ldots, P_{i-n}^n) \quad n = 1, 2, \ldots, N \tag{4}$$

Equation (5), which accounts for period T of the previous samples, yields the AAD of each array at *sample i*.

$$AAD_i^n = (|P_i^n - m_i^n|, \left|P_{i-1}^n - m_i^n\right| \ldots, |P_{i-w}^n - m_i^n|) \tag{5}$$

Each data set's standard deviation, δ_i^n, can be found by multiplying its AAD by factor $k = 1.4826$, which can be found through a relationship with the Gaussian error function.

$$\delta_i^n = k \times AAD_i^n \tag{6}$$

A three-sigma filter is applied to each measured value. If there is a discrepancy between the measured power and its average, the measured value is regarded as an outlier and is returned; otherwise, the measured value is kept. Equation (7) is used to determine the filtered measured value, Pf_i^n.

$$Pf_i^n = \begin{cases} P_i^n, |P_i^n - m_i^n| \leq 3.\delta_i^n \\ m_i^n, \left|P_i^n - m_i^n\right| > 3.\delta_i^n \end{cases} \tag{7}$$

2) SYSTEMATIZATION

Every measured value that undergoes filtering based on prior measurements is adjusted for normality by the PV array. Prioritizing each array's current generation according to its maximal capacity is crucial. P_{nom}^n, the total capacity of each array, is found using equation (8).

$$P_{nom}^n = Qs^n.\, QP^n.\, P_{pan}^n \tag{8}$$

QP^n is the number of panels per array, P_{pan}^n represents the power provided by each panel per array, and Qs^n is the number of strings per array. Equation (9), when applied to the filtered measured value, can normalize it.

$$P_{norm}^n = \frac{Pma_i^n}{P_{nom}^n} \tag{9}$$

Afterward, equation (10) can be used to calculate each array's performance.

$$P_{npfi}^n = \frac{Pnorm_i^n}{\max(Pnorm_i^1, Pnorm_i^2, \ldots, Pnorm_i^N} \tag{10}$$

3) THE ACTIVATION OF THE GENERATION PROCESS

The AAD result provides a useful illustration of the data's variability around its average value. It is important to include the final threshold for evaluation of shaded panels, even though the standard deviation of its value might be utilized as a threshold. The limit trigger (Lim_i) of 0.95 is suggested by this algorithm. The optimal threshold value of 0.95 is chosen to ensure a conservative approach to identifying underperforming PV arrays, aiming to minimize the risk of false positives while effectively triggering restart conditions for arrays operating below expected levels. The electricity generated by the PV panels is distributed normally around the average, with three sigmas representing 99.9% of the population:

$$Lim_i = \max(0.95, m_{npfi} - 3\delta npfi) \tag{11}$$

An underperforming PV array is one whose performance falls short of the predetermined threshold. Equation (12) represents the triggering flag of each inverter ($flag_i^n$).

$$flag_i^n = \begin{cases} 0, & Pnpfi_i^n \geq Lim_i \\ 1, & Pnpfi_i^n < Lim_i \end{cases} \tag{12}$$

Equation (13) can be used to represent the ultimate trigger signal while accounting for changes in sun irradiation during the day. Only when the homogenized generation is larger than or equal to 0.05 $p.u.$ does the flag get raised.

$$f_i^n = \begin{cases} flag_i^n, & \max(Pnorm_i^n) \geq 0.05 \\ 0, & \max(Pnorm_i^n) < 0.05 \end{cases} \quad (13)$$

The controller notifies the inverter of the restart condition by sending it the last triggering signal when it determines that the PV array is not operating as expected. PV farms can utilize this for monitoring purposes. The PV array may be deemed permanently shaded or faulty if it exhibits poor performance for a few hours.

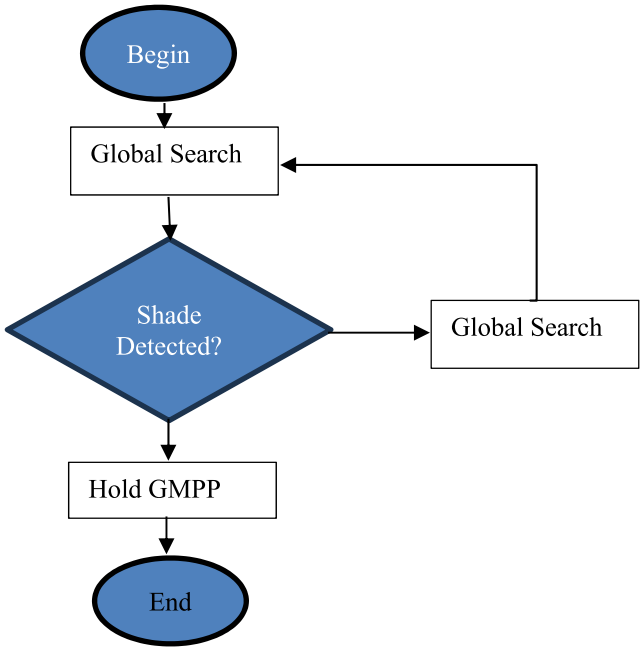

FIGURE 2. Stat-up condition in GMPP search.

C. EXPECTATION CONJUGATE GRADIENT

The Expectation-Conjugate-Gradient (ECG) method is an optimization algorithm that combines the concepts of expectation and conjugate-gradient optimization techniques. It is particularly useful for solving optimization problems involving large-scale data or computationally intensive objectives. The ECG algorithm iteratively updates the search direction and step size to minimize the expected objective function. It belongs to the conjugate-gradient family, which offers efficient solutions for linear systems and optimization tasks. ECG specifically addresses the minimization of quadratic functions when the underlying probability distribution is unknown, making it suitable for problems involving probabilistic models and expectation maximization.

The core objective of ECG is to iteratively update a sequence of vectors to converge towards the optimal solution of the quadratic function. The algorithm incorporates the expectation operator, which computes the expected value of a function based on a given probability distribution. This integration of probabilistic information allows ECG to navigate the optimization process effectively. To accomplish optimization, ECG iteratively minimizes the expected quadratic function and its conjugate. In each iteration, it calculates the expected gradient of the quadratic function by integrating the product of the gradient and the probability density function across the distribution. While this computation can be computationally demanding for complex distributions, it remains tractable for certain families of distributions.

ECG leverages the conjugate-gradient technique for efficient optimization. This method exploits the conjugate directions of a matrix to solve linear systems swiftly. By utilizing conjugacy properties, ECG determines optimal step sizes and directions at each iteration, leading to rapid convergence and reducing the need for numerous function evaluations. The convergence properties of ECG are favorable, ensuring that the algorithm reaches a local minimum of the expected quadratic function. However, the rate of convergence can be influenced by factors such as problem conditioning and the choice of initial values. Effective initialization and preconditioning techniques can mitigate these factors and enhance convergence.

ECG finds applications in diverse domains, including machine learning, image processing, and data analysis. It proves particularly valuable when tackling complex optimization problems involving probabilistic models. By incorporating the expectation operator and leveraging the conjugate-gradient technique, ECG provides an efficient and effective solution for a wide range of problems. Nevertheless, ECG has certain limitations. It assumes an unknown underlying probability distribution, requiring estimation during the optimization process. This estimation can introduce additional computational complexity and demand significant resources. Additionally, the algorithm's performance can be sensitive to the selection of optimization parameters and the presence of data noise.

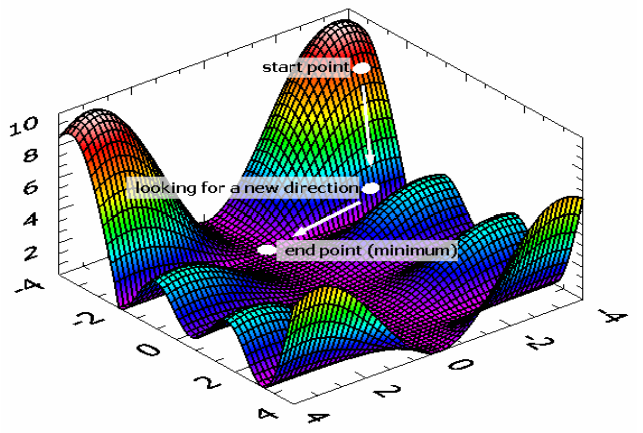

FIGURE 3. ECG direction determination.

The ECG algorithm is an iterative optimization method used to find the minimum of a function. It is often employed

in the context of variational inference for approximating posterior distributions in probabilistic models. Below is the basic outline of the ECG algorithm:

Compute the gradient of the function $f(x)$ at the current parameter xk : $gk - \nabla f(xk)$.

Compute the natural gradient $g'k$ using the expectation of the gradient of the log-likelihood with respect to a variational distribution (which serves as a proxy for the true posterior): $g'k - Eqk[\nabla logp(x, \theta) \mid xk]$,

Where qk is the current variational distribution and θ represents other model parameters that x depends on.

Compute the search direction dk as a solution to the linear equation: $(I - \alpha kBk)dk - g'k$,

where αk is the step size (learning rate) at iteration k, and Bk is the approximation of the Fisher information matrix, which is positive definite and approximated from the current variational distribution.

Update the parameter vector using the computed search direction: $xk + 1 - xk + \alpha kdk$.

Finally, Increment the iteration counter: $k - k + 1$.

ECG Control Strategies in the Application of Power Quality Improvement – The ECG algorithm emerges as a potent tool for harmonic mitigation within Grid-Tied PV systems by regulating the interfacing inverter. In the pursuit of optimizing harmonic content in the PV system, ECG provides a unique solution by iteratively adjusting the inverter's control parameters. The algorithm strategically leverages the expectation operator to minimize the expected quadratic function representing harmonic distortions. This integration allows the ECG algorithm to effectively explore the parameter space, enhancing the inverter's adaptability to the dynamic and probabilistic nature of grid harmonics. The conjugate-gradient technique further refines this process by efficiently determining optimal step sizes and directions, ensuring a swift convergence towards an optimized inverter configuration that mitigates harmonic distortions in the system.

The application of the ECG algorithm in the control strategy of interfacing inverters presents several noteworthy advantages for Grid-Tied PV systems. By dynamically optimizing the inverter parameters, ECG enables real-time adaptation to varying grid conditions and PV power outputs, contributing to improved harmonic mitigation performance. The algorithm's conjugate-gradient approach minimizes the need for extensive function evaluations, thereby reducing computational burden and enhancing overall efficiency. Moreover, the probabilistic modeling incorporated in ECG allows for a more robust and adaptive response, accommodating uncertainties associated with grid harmonic characteristics. In essence, the ECG algorithm adds significant value to Grid-Tied PV systems by providing a sophisticated and efficient solution for harmonic mitigation, fostering enhanced power quality and stability.

The benefits derived from implementing the ECG algorithm in harmonic mitigation for Grid-Tied PV systems extend beyond mere technical improvements. The enhanced power quality resulting from optimized inverter control contributes to a more reliable integration of renewable energy sources into the grid, minimizing the risk of disruptions and ensuring sustained energy supply. Furthermore, the improved efficiency in harmonic mitigation translates into reduced wear and tear on electrical components, potentially extending the operational lifespan of the PV system. The algorithm's adaptability to dynamic grid conditions aligns with the evolving nature of renewable energy sources, positioning the ECG-based control strategy as a valuable asset in the pursuit of sustainable and resilient power infrastructures.

Consequently, the implementation of the proposed inner current control strategy ensures an elevated standard of current quality. This approach relies on the utilization of three-phase grid currents as its primary input, with computations streamlined through the application of Synchronous Reference Frame (SRF) theory, as discussed in [28]. The three-phase grid currents (I_{ga}, I_{gb}, I_{gc}) undergo sensing and transformation into the d-q axis frame.

Upon transformation, the d-q components, denoted as I_d and I_q, are computed using the following expressions:

$$I_d = \frac{2}{3}(I_{ga}sin\omega t + I_{gb}\left(\omega t - \frac{2\pi}{3}\right) + I_{gc}sin(\omega t + \frac{2\pi}{3}) \tag{14}$$

$$I_q = \frac{2}{3}(I_{ga}cos\omega t + I_{gb}\left(\omega t - \frac{2\pi}{3}\right) + I_{gc}cos(\omega t + \frac{2\pi}{3}) \tag{15}$$

Subsequently, the transformed d-q components are reverted back to three-phase reference voltages and then forwarded to the Pulse Width Modulation (PWM) stage. In this process, PWM generates pulses corresponding to the reference voltage signals, subsequently controlling the VSI IGBTs in the system. This intricate control mechanism ensures precise manipulation of the inverter output, maintaining optimal current quality in the grid-tied system.

D. ENHANCED DSOGI-PLL

Addressing the imperative need for a precise and swift approximation of grid information within grid-tied PV systems, Phase-Locked Loop (PLL) schemes have been employed due to their recognized superiority in performance, as noted in [29]. The widely adopted DSOGI-PLL stands out for its structural simplicity, especially in three-phase grid synchronization, as corroborated in [29]. However, the conventional DSOGI-PLL grapples with substantial performance degradation under unbalanced grid conditions and distortions. Moreover, it exhibits drawbacks such as sluggish response times, considerable frequency overshot, and limited disturbance rejection capabilities.

This paper introduces an enhanced DSOGI-PLL, denoted as EDSOGI-PLL, designed to surmount the aforementioned limitations, and elevate overall performance. Illustrated in Figure 4, the proposed scheme employs a control loop

based on the quasi-type 1 (QT1) strategy. Notably, the Savitzky-Golay Filter (SGF) replaces the conventional moving average filter (MAF) within the DSOGI-PLL to enhance dynamic performance. An SGF is a type of smoothing filter particularly useful for noise reduction in time-series data. It preserves important features while removing noise. Positioned on the feedforward path, the SGF plays a pivotal role in augmenting phase and frequency synchronization response time, effectively eliminating frequency overshot.

The SGF stands out as a versatile and powerful filtering tool due to its unique advantages over other filters. It excels in simultaneously smoothing data while preserving crucial signal features, making it ideal for applications where fidelity to the original signal is paramount. The SGF's capability to perform both smoothing and differentiation in a single operation is particularly valuable for extracting relevant information from noisy data. Its adaptability with variable window sizes ensures flexibility in handling signals with diverse characteristics. Noteworthy is its ability to minimize phase shift, making it suitable for applications requiring accurate temporal relationships. The SGF's robustness to outliers, computational efficiency, ease of implementation, and adaptability to unevenly sampled data further enhance its appeal across a broad range of scientific and engineering domains, solidifying its position as a preferred filter for applications demanding precision and versatility.

In addition to its structural modifications, the proposed EDSOGI-PLL undergoes a meticulous parameter design procedure to bolster its disturbance rejection capabilities. It is crucial to note that the standard DSOGI-PLL, expressed as:

$$D_{PLL} = \frac{\omega_p}{s + \omega_p} \tag{16}$$

where ω_p denotes the cut-off frequency, and ω_p is chosen as $k\omega_f/2$, with ω_f representing the fundamental grid frequency, serves as the foundational framework for the enhanced scheme.

The utilization of DSOGI-PLL, augmented by the SGF, provides several advantages. The enhanced scheme addresses the limitations of its conventional counterpart, delivering improved performance in unbalanced grid scenarios and distorted conditions. The replacement of the moving average filter with the SGF contributes to enhanced dynamic response and eliminates issues like frequency overshot. Additionally, the meticulously designed parameters enhance disturbance rejection capabilities, ensuring the proposed EDSOGI-PLL remains robust in real-world grid-tied PV system applications. This innovative approach signifies a substantial advancement in achieving precision and rapid grid information approximation, thereby contributing to the overall reliability and efficiency of grid-tied PV systems.

The selection of the window length (L_w) in SGF filters plays a pivotal role and is determined based on the anticipated harmonic content within the grid system. Specifically, the dominant disturbances arising from the 3rd, 5th, 7th, 11th, and 13th harmonics are crucial considerations in this context.

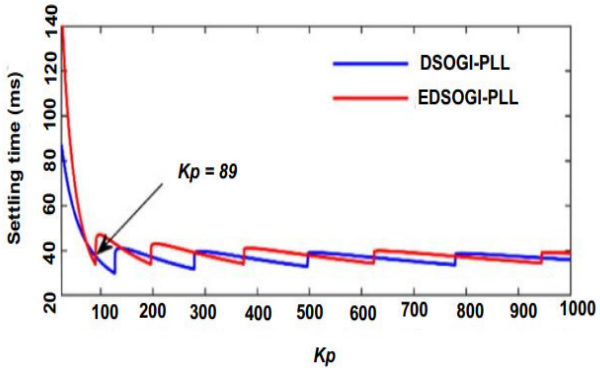

FIGURE 4. Evaluation of EDSOGI-PLL and DSOGI-PLL in the presence of phase/frequency jumps.

In this paper, the period of the grid voltage (T) is deliberately set to $T/7$, given that the harmonics content of interest often occurs within this timeframe. The adjustability of (L_w) in SGF and the controller parameter (k_p) follows the calculation of $\omega_p$in the Digital Second-Order Generalized Integrator Phase-Locked Loop (DSOGI-PLL). The determination of k_p involves establishing the open-loop transfer function, denoted as G_ol(s), where:

$$G_{ol}(s) = \frac{\Delta\emptyset^{+}(s)}{\emptyset_e(s)} = \left(\frac{D_{PLL}(s)}{1 - D_{PLL}(s).SGR(s)}\right)\left(SGR(s) + \frac{k_p}{s}\right) \tag{17}$$

Subsequently, the phase-tracking-error transfer function ($G_e(s)$) is derived using Equation (18), representing the relationship between $\emptyset_e(s)$ and $\Delta\emptyset^{+}(s)$.

$$G_e(s) = \frac{\emptyset_e(s)}{\Delta\emptyset_i(s)} = \left(\frac{1}{1 - G_{ol}(s)}\right) \tag{18}$$

The plotting of the 1% settling time of $G_e(s)$ under a phase/frequency jump scenario, utilizing a specified k_p value of 89, reveals that the SGF showcased a diminished settling time, indicative of a swifter and more efficient response. This outcome suggests that the proposed Enhanced DSOGI-PLL, configured with a k_p value of 89 and employing the SGF, demonstrates favorable dynamic performance, rapidly adapting to variations in the grid system. Such adaptability contributes significantly to the system's reliability and precision in real-world applications, affirming its suitability for demanding operational environments.

Figure 5 visually depicts the proposed Enhanced DSOGI-PLL (EDSOGI-PLL), emphasizing its high precision in approximation. Comparative analysis, as detailed in Table 1, highlights that the proposed method exhibits the lowest frequency and phase overshot in contrast to the conventional DSOGI-PLL. Additionally, the proposed EDSOGI-PLL achieves a dynamic rapid settling time of 15ms within 2 cycles, indicating its efficiency in responding to dynamic changes in the grid system. The comparison presented in Table 1 provides insightful metrics for evaluating the superiority of the proposed approach.

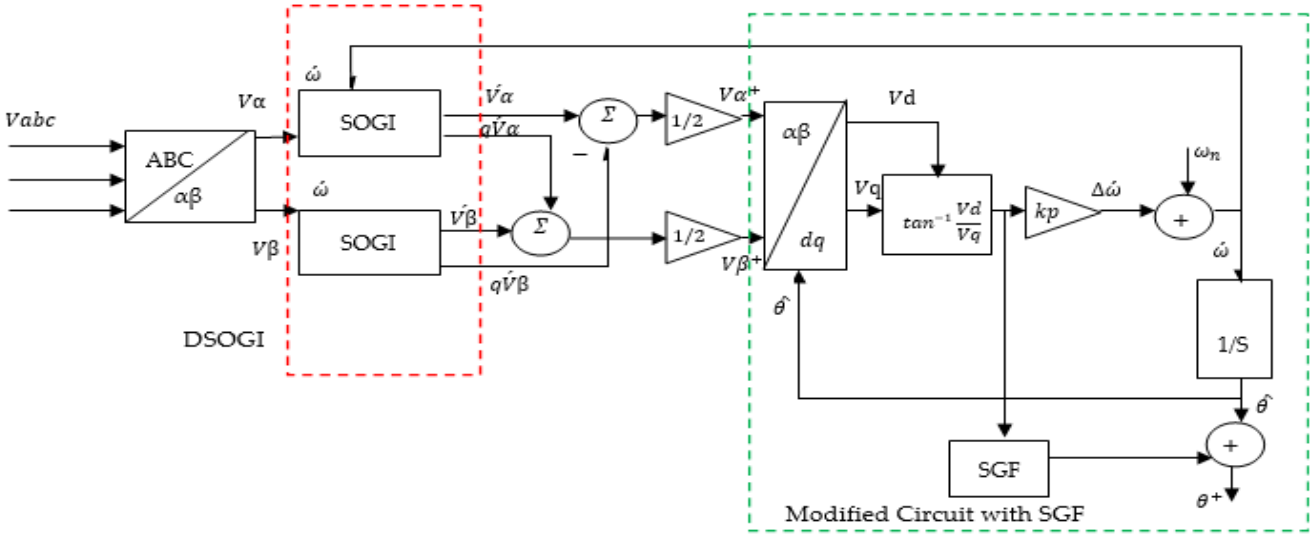

FIGURE 5. Schematic diagram for the envisioned EDSOGI-PLL.

Notably, the settling time of the proposed EDSOGI-PLL is measured at 15ms, demonstrating a substantial improvement over the standard DSOGI-PLL's settling time of 35ms. This reduction in settling time signifies the enhanced rapid response of the proposed EDSOGI-PLL to dynamic changes in the grid system, contributing to its superior dynamic performance.

Furthermore, the frequency overshoot for the proposed EDSOGI-PLL is notably lower at 1% compared to the standard DSOGI-PLL's higher frequency overshoot of 35%. This implies that the proposed EDSOGI-PLL achieves more accurate frequency tracking with minimal overshoot, enhancing its precision in maintaining synchronization with the grid frequency. Although there is a marginal increase in phase overshoot for the proposed EDSOGI-PLL (9°) compared to the standard DSOGI-PLL (8°), this difference is relatively minor. Overall, the results suggest that the proposed EDSOGI-PLL outperforms the standard DSOGI-PLL in terms of settling time and frequency overshoot, highlighting its superiority in dynamic response and frequency tracking accuracy, which are critical attributes in grid-tied PV systems.

The discussed adjustment to the circuit has improved the dynamic performance of the EDSOGI-PLL. When high-order harmonics and an uneven grid voltage are present, the grid reacts swiftly. It has been demonstrated to give the ability to extract phase information precisely and quickly from the grid fundamental wave. The scheme's drawback, however, is that low order harmonics are a problem. The technique needs to be enhanced in order to acquire more exact grid voltage phase information because it's necessary to lessen the influence of low order harmonics.

The subsequent phase of the contribution involves the proposition of an augmented enhancement to the DSOGI-PLL scheme. This augmentation entails the incorporation of a Sequential Cascaded Harmonic Blocking Module (HBM) with the aim of precisely mitigating the emergence of low-order harmonics. The schematic diagram depicting the proposed EDSOGI-PLL, integrating the sequential cascaded HBM, is delineated in Figure 6.

The 3-phase voltage can be described using equation (19) under the conditions of more erratic low order harmonics in the power systems grid.

$$\begin{bmatrix} V_a \\ V_b \\ V_c \end{bmatrix} \sqrt{2}U_{+1} \begin{bmatrix} Cos(\omega_o t + \varphi_{+1}) \\ Cos(\omega_o t + \varphi_{+1} - \frac{2\pi}{3}) \\ Cos(\omega_o t + \varphi_{+1} + \frac{2\pi}{3}) \end{bmatrix} + \sqrt{2}U_{-1} \begin{bmatrix} Cos(-\omega_o t + \varphi_{+1}) \\ Cos(-\omega_o t + \varphi_{-1} - \frac{2\pi}{3}) \\ Cos(-\omega_o t + \varphi_{-1} + \frac{2\pi}{3}) \end{bmatrix} \sum U_n \begin{bmatrix} Cos(n\omega_o t + \varphi^n) \\ Cos(n\omega_o t + \varphi^n - \frac{2\pi}{3}) \\ Cos(n\omega_o t + \varphi^n + \frac{2\pi}{3}) \end{bmatrix} \tag{19}$$

where U_n and φ^n denotes the amplitude and initial phase of the *nth* harmonics. Then the transformation is represented by equation (20).

$$V_{\alpha\beta} = \begin{bmatrix} U_\alpha \\ U_\beta \end{bmatrix} = U^+_{\alpha\beta} + U^-_{\alpha\beta} + \sum U^n_{\alpha\beta} \tag{20}$$

Put the resonance frequency of DSOGI-PLL to grid frequency 0 and utilize the $V_\alpha \& V_\beta$ as input signals of the integrator to determine the output signal that contains positive and negative sequence and *nth* harmonic content. It is represented by equation (21)-(22).

$$\begin{cases} V'_\alpha = V^+_\alpha + V^-_\alpha + V^{n*}_\alpha \\ qV'_\alpha = V^+_\beta + V^-_\beta + \frac{1}{n}V^{n*}_\beta \end{cases} \tag{21}$$

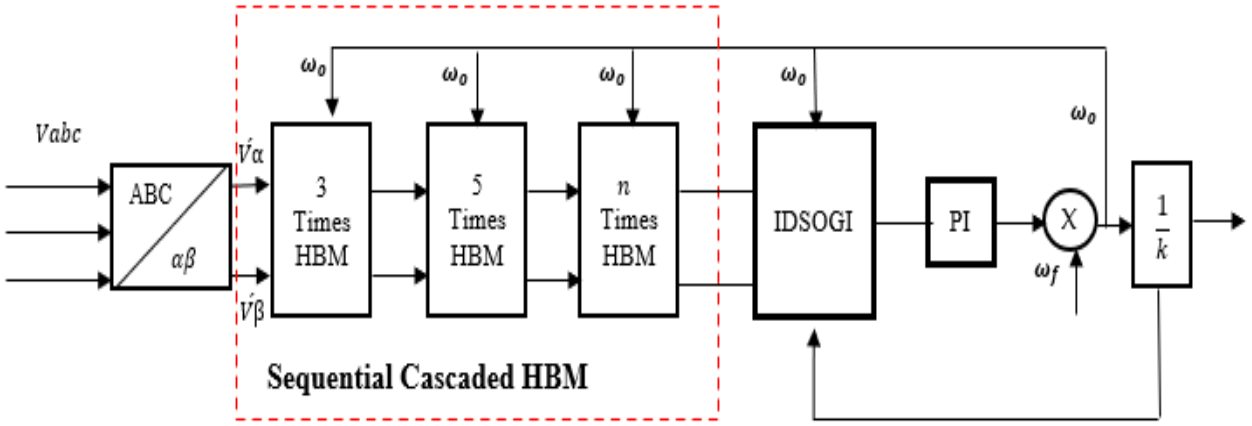

FIGURE 6. Proposed sequential cascaded HBM scheme.

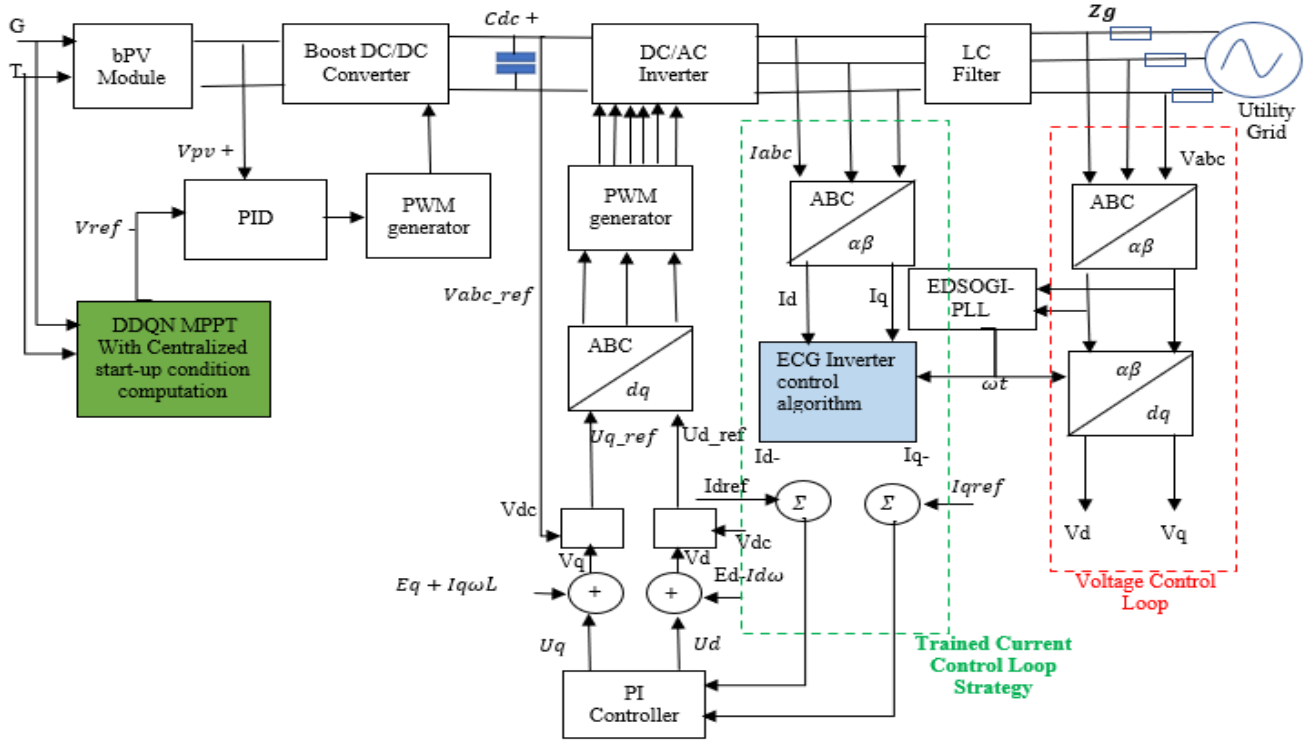

FIGURE 7. Proposed integrative Grid-tied photovoltaic system diagram.

$$\begin{cases} V'_\beta = V^+_\beta + V^-_\beta + V^{n*}_\beta \\ qV'_\beta = -V^+_\alpha + V^-_\alpha - \dfrac{1}{n}V^{n*}_\alpha \end{cases} \tag{22}$$

Thus,

$$V^{n*}_\alpha = |D||\,\omega = n\omega_o U^n Cos(n\omega_o t + \varphi^n + <D|\omega = n\omega_o \tag{23}$$

$$V^{n*}_\beta = |D||\,\omega = n\omega_o U^n Cos(n\omega_o t + \varphi^n + <D|\omega = n\omega_o \tag{24}$$

The integrator corresponds to the output as two component frequencies with a 90-degree phase difference, however equations (21) and (22) both modify the extremum and phase position of the harmonic content. The term ''positive voltage sequence component'' refers to both the positive and negative sequence components (PNSC). Equation can be used to represent the PNSC (25).

$$\begin{cases} V^n_\alpha = \dfrac{1}{n}V^+_\alpha + qV'_\alpha = (\dfrac{1}{n}-1)V^+_\alpha + (\dfrac{1}{n}+1)V^-_\alpha \\ V^n_\beta = \dfrac{1}{n}V^+_\beta - qV'_\beta = (\dfrac{1}{n}-1)V^+_\beta + (\dfrac{1}{n}+1)V^-_\beta \end{cases} \tag{25}$$

The modified two-phase voltage is shown to reduce the harmonic content and only contain the PNSC with an

amplitude change by comparing equations (21) and (22). The large low order harmonics can be expressed using equation (26).

$$V_{\beta}^{n} = \begin{bmatrix} V_{\alpha}^{n} \\ V_{\beta}^{n} \end{bmatrix} = (\frac{1}{n} - 1)V_{\alpha\beta}^{+} + (\frac{1}{n} - 1)V_{\alpha\beta}^{-} + (\frac{1}{n} - \frac{1}{h})V_{\alpha\beta}^{h} \tag{26}$$

Equation (26) uses the HBM technique to reduce the target subharmonic content. The amplitude of two orthogonal harmonic content in equations (21) and (22) is only linked to the number of harmonics. As a result, HBM is used to filter out the arising low order harmonics. Equation (21) demonstrates that since the coefficients are multiplied by the PNSC of the voltage corresponding to each stage of the HBM when the voltage harmonics are removed. Before the Park's transformation, a gain link is applied to correct the component amplitude, and the gain coefficients are expressed as (27).

$$\begin{cases} k = \dfrac{1}{\pi(\frac{1}{n}-1)} \\ k' = \dfrac{1}{\pi(\frac{1}{n}-1)} \end{cases} \tag{27}$$

E. PROPOSED INTEGRATIVE GRID-TIED PV SYSTEM CONFIGURATION

Figure 7 illustrates the qualitative aspects of power generation and transmission within a grid-connected solar PV system, incorporating a novel DDQN MPPT algorithm with a centralized start-up condition and an ECG system enhanced by an EDSOGI-PLL modified using the SGF algorithm. The proposed system features a two-stage PV system contributing power to the utility grid, employing 1STH-215-P Soltech bifacial PV panels with specifications detailed in Table 2. These bifacial PV modules are configured in a fixed-tilt arrangement. The DDQN MPPT algorithm, optimized through centralized start-up computation, is introduced to attain the optimal DC link voltage at the common DC bus under PSC. This integrative MPPT algorithm synergizes the advantages of DDQN and centralized start-up computation, enhancing overall performance within a unified framework. Capable of discerning scheduled or underperforming PV arrays, the algorithm globally searches specified arrays after a trigger signal, optimizing energy capture. The Boost DC/DC converter, designed with consideration for DC link capacitor specifications, steps up the DC link voltage to match the DC/AC inverter requirements. The DC-link capacitor functions as an energy storage unit and aids in mitigating voltage ripples across the PV array [30].

The DC/AC inverter, connected to the utility grid via an LC filter and step-up transformer, converts DC to AC power while the LC filter minimizes high-order harmonics. The novel ECG integrated with the EDSOGI-PLL, modified using SGF, controls the grid interfacing inverter, thereby enhancing power quality. The ECG-DSOGI-PLL with SGF strategy employs a dual-loop power flow controller, encompassing outer-loop voltage and inner-loop current controllers. This involves sensing three-phase currents, converting them to direct-quadrature (d-q) components using Parks Transformation, and determining three-phase reference voltages. These reference voltages generate firing angle signals for the PWM generator, driving the inverter IGBT's gates to produce a pure sinusoidal waveform. The EDSOGI-PLL ensures synchronization between the grid and inverter. Notably, this proposed grid-integrated PV system accommodates both linear and nonlinear loads. The integrative scheme benefits from improved MPPT efficiency, enhanced power quality, and the ability to discern and optimize PV arrays dynamically, thereby maximizing energy capture and grid performance in diverse conditions.

TABLE 2. Specification of the proposed system.

Parameters	Value
PV module	Bifacial (1STH-215-P)
Nominal Power	2 kW
Vmpp	223.5V
Impp	9.3A
Number of series modules (Ns)	10
Series resistance (Rs)	0.39383Ω
Shunt resistance (Rsh)	313.3991Ω
L1 (DC link inductor)	100 mH
C1	100 µF
C2	100 µF
Ro	20 Ω
C3 (DC Link Capacitor)	$1100\mu F$
DC link Voltage	280VDC
LC Filter	$L = 4.8mH\ ; C = 4.3\mu F$
Controller sampling frequency	20kHz
Sampling period	5µs
Albedo	30
GCR (%)	35
Collector height (m)	2.1
Collector width (m)	3.75
Collector azimuth (°)	0
Tilt (°)	30
Inverter rated power	2kVA
Inverter input VDC	120Vdc-290Vdc
Inverter Output VAC	380Vac (±5%) – 3 phase
Grid nominal voltage	380Vac
Grid nominal current	25A
Grid local power	1.7kW
Grid nominal Frequency	50Hz

IV. SYSTEM SETUP

This section illustrates the configuration of the proposed bifacial Photovoltaic (bPV) system with a fixed tilt design, emphasizing a meticulous installation approach aimed at optimizing energy yield from bifacial modules [30]. The

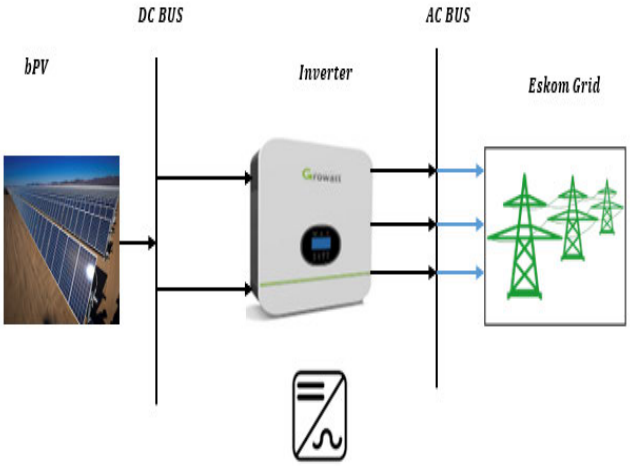

FIGURE 8. Proposed integrative Grid-tied photovoltaic system architecture.

system is defined with a fixed tilt angle of 30 degrees and a constant albedo of 30% for both modules. To achieve the optimal system configuration, a ground coverage ratio (GCR) of 35% is chosen, along with a collector height and width of 2.1m and 3.75m, respectively. The simulation assesses energy yield, bifacial gain, and tracking gain for this fixed-tilt setup, utilizing the Johannesburg, Alberton dataset from South Africa. The region exhibits an anticipated specific production of 1753 kWh/kWp per year and an expected Annual Global Horizontal Irradiation of 2,061 kWh/m^2, surpassing benchmarks set by other commercial PV projects in South Africa. Detailed specifications of the proposed system can be found in Table 2.

The proposed PV system, centered around the bifacial modules, notably integrates the 1STH-215-P model, boasting a 2 kW nominal power rating. The DC link voltage is precisely set at 280VDC, complemented by the inclusion of an LC filter to enhance system performance. Operating at a high precision, the controller orchestrates a sampling frequency of 20kHz, with a minimal sampling period of 5μs. The inverter, a pivotal component in the system, is rated at 2kVA, showcasing its capability to handle input voltages within the range of 120Vdc to 290Vdc. Its output is a robust 380Vac (±5%), presented in a three-phase configuration to ensure efficient power delivery. Key grid parameters include a nominal voltage of 380Vac, a nominal current of 25A, and a local power output of 1.7kW. Notably, the system seamlessly aligns with the standard grid nominal frequency of 50Hz. Figure 8 serves as a demonstrative visual representation of the system's architecture and functionality, providing a comprehensive overview of its key components and interconnections.

This paper encompasses four (4) distinct case studies designed to assess and analyze the performance of the proposed system. By examining multiple cases, this can assess the system's robustness, efficiency, and adaptability across various environmental and operational parameters.

A. CASE STUDY 1 – FIXED TILT APPROACH

This segment outlines the proposed configuration for the bifacial Photovoltaic (bPV) system, employing a fixed tilt design aimed at optimizing energy yield from the bifacial modules. The simulation is conducted to assess energy yield, bifacial gain, environmental analysis and tracking gain for this fixed-tilt configuration, utilizing the Johannesburg dataset in South Africa. The chosen location boasts an anticipated specific production of 1753 kWh/kWp annually and an expected Annual Global Horizontal Irradiation of 2,061 kWh/m^2, surpassing benchmarks set by other commercial PV projects in South Africa. Figure 9 provides a visualization of the solar irradiance path and Iso-shading diagram for the proposed location.

The average annual low temperature is recorded at 20.5°C, with December identified as the warmest month at an average temperature of 25°C, while July stands as the coldest month at 18°C. Detailed temperature statistics from January 2009 to January 2023 are presented in Figure 10, indicating a maximum recorded temperature of 29°C and a minimum of 1°C, based on NASA's weather dataset [31]. Furthermore, the average monthly relative humidity ranges from 36% in July to 90% in January over the same period.

Figure 11 visually depicts the global photovoltaic power potential, with a specific emphasis on Johannesburg in the Gauteng province of South Africa. The city stands out as a strategic location for solar energy harvesting due to its unique geographical positioning and ample solar exposure. This case study is substantiated by the meticulous modeling and simulation conducted through advanced tools, including PV Syst 7.4, HOMER, and MATLAB R2023 Software.

The performance of the algorithms is evaluated using three key metrics: Root Mean Squared Error (RMSE), Mean Absolute Error (MAE), and Mean Squared Error (MSE). These metrics, calculated using equations (28) to (30), provide quantitative measures of the algorithm's accuracy and effectiveness in predicting outcomes.

$$MSE = \frac{1}{N}\sum_{i=1}^{N}(y-t)^2 \tag{28}$$

$$RMSE = \sqrt{\frac{1}{N}\sum_{i=1}^{N}(y-t)^2} = \sqrt{MSE} \tag{29}$$

$$MAE = \frac{1}{N}\sum_{i=1}^{N}|(y-t)| \tag{30}$$

B. CASE STUDY 2 – DYNAMIC MPPT ALGORTIHM PERFORMANCE UBDER PSC

In Case Study 2, a notable variation in solar insolation levels, transitioning from G1 at $1000W/m^2$ to $G2 = 855W/m^2$, $G3 = 966W/m^2$, and $G4 = 925W/m^2$ as shown in Table 3, is employed to assess the efficacy of the proposed DDQN with centralized start-up condition MPPT algorithm under PSC. The PV module temperature undergoes changes from T1 = 23°C, T2 = 27°C, T3 = 28°C, and T4 = 15°C

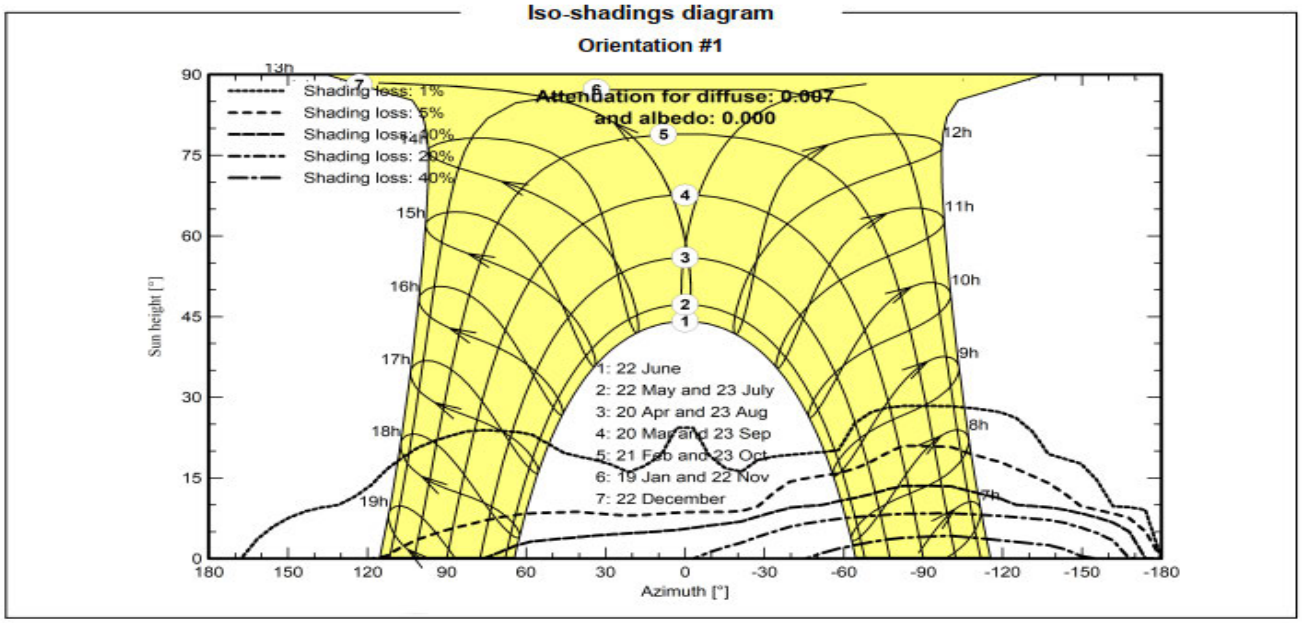

FIGURE 9. Solar Sun path and Iso-shading diagram [31].

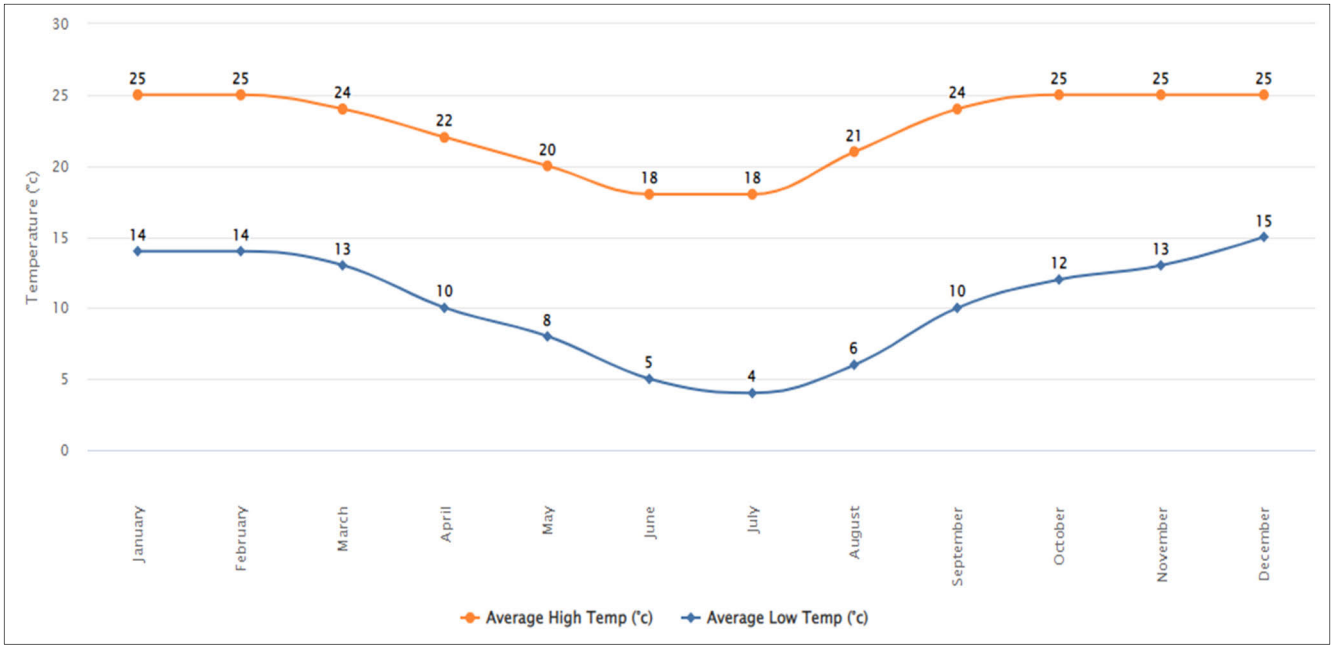

FIGURE 10. Johannesburg monthly average temperature [31].

during this investigation. To ensure a rapid dynamic response and maintain a stable DC current within specified limits for the inverter, the DC link inductor is kept constant at 100mH. The performance of the proposed DDQN MPPT algorithm is evaluated under a linear load of 1.7 kW to measure the Total Harmonic Distortion (THD) in the grid. The THD for voltage and current is individually calculated through equations (31) and (32), respectively. The THD level is quantified using Fast Fourier Analysis (FFT) in accordance with the IEEE 519 standard.

$$THD_V = \frac{\sqrt{\sum_{n=2}^{N} V_{\Pi}^2}}{V_1} \times 100\% \tag{31}$$

$$THD_I = \frac{\sqrt{\sum_{n=2}^{N} I_{\Pi}^2}}{I_1} \times 100\% \tag{32}$$

where THD_V is the system voltage total harmonic distortion and THD_I system current total harmonic distortion.

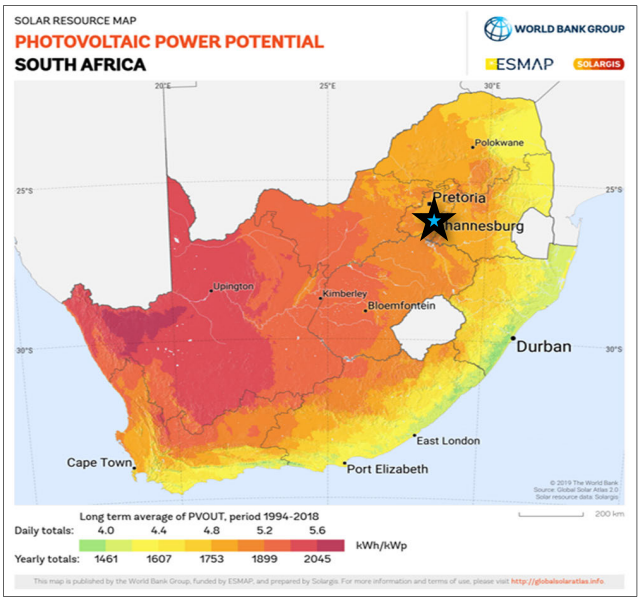

FIGURE 11. Photovoltaic power potential for South Africa, Johannesburg [31].

TABLE 3. Specification of the proposed system.

Case Studies	Irradiance (W/m^2)	Temperature (°C)	DC-Link Inductor	Load
C2	G1=1000 G2=855 G3=966 G4=925	T1=25 T2=27 T3=28 T4=15	L=100mH	1.5kW
C3	G1=950 G2=800 G3=860 G4=790	T1=28 T2=29 T3=31 T4=32	L=90mH	1.7kW to 1.9kW
C4	G1=850 G2=640 G3=670 G4=590	T1=24 T2=20 T3=18 T4=14	L=70mH	1.7kW to 2kW

Ultimately, the substantial impact of elevated THD levels contributes to a degradation in the Power Factor (PF) of the system, resulting in an escalation of customer tariffs. The system PF is determined using equation (33) with reference to the IEEE standard 1459 [32].

$$PF = \frac{1}{\sqrt{1 + \left(\frac{THD\%}{100}\right)^2}} \tag{33}$$

C. CASE STUDY 3 - EXPLORING PATTERNED SOLAR IRRADIANCE VARIATION

Within the confines of Case Study 3, our objective is to elucidate the intricacies of Patterned Solar Irradiance Variation (PSC Pattern 2) while scrutinizing the efficacy of a novel DDQN. This scrutiny is conducted amidst dynamic alterations in solar irradiance levels and module temperatures, contemplating four distinct scenarios $G1 = 950W/m^2$, $G2 = 800W/m^2$, $G3 = 860W/m^2$, and $G4 = 790W/m^2$. Simultaneously, the module temperatures exhibit variance with T1 = 28°C, T2 = 29°C, T3 = 31°C, and T4 = 32°C.

The experimental complexity is heightened by the deliberate reduction of the DC link inductor to $90mH$. Additionally, an innovative non-linear load is introduced, characterized by a power ramp-up trajectory from $1.7kW$ *to* $1.9kW$ within the temporal bounds of $t = 0.3 - 0.6s$. This non-linear load integration serves as a conduit for the evaluation of THD levels pertinent to the proposed ECG strategy. The quantification and assessment of THD are executed through the application of FFT methodologies, aligning with the rigorous specifications articulated by the IEEE 519 standard.

Beyond the realms of THD scrutiny, due consideration is accorded to the measurement of PF under the auspices of the IEEE 1459 international standard for power quality analysis. This multifaceted analytical approach ensures a comprehensive evaluation of the proposed DDQN, fostering nuanced insights into its resilience and efficacy within the dynamic context of solar power generation. The richness and depth of this investigation contribute substantively to the scholarly discourse on advanced control strategies in renewable energy systems [33], [34].

D. CASE STUDY 4 - ENHANCING POWER QUALITY IN LOW IRRADIANCE ENVIRONMENTS

In the conclusive Case Study 4, a sophisticated Patterned Solar Irradiance Variation (PSC) pattern is introduced, presenting a challenging scenario for the solar panel. The solar irradiance levels in this intricate pattern are notably low, specifically denoted as $G1 = 850W/m^2$, $G2 = 640W/m^2$, $G3 = 670W/m^2$, and $G4 = 590W/m^2$. Concurrently, the module temperature undergoes fluctuations, transitioning from T1 = 24°C T2 = 20°C, T3 = 18°C, and T4 = 14°C.

To intensify the complexity of the study, adjustments are made to the DC link inductor, reducing it to 70 mH. Moreover, a non-linear load is integrated into the system, undergoing a power ramp-up from $1.7kW$ *to* $2kW$. The primary objective of this configuration is to assess the performance of the propose MPPT and inverter control strategies in enhancing the quality of power. In this case, QRNN control strategy is also introduced to validate the effectiveness of the proposed DDQN algorithm. This evaluation is conducted utilizing the FFT toolbox, providing a comprehensive analysis of the system's response to challenging environmental conditions. The outcomes of this investigation contribute valuable insights into the robustness and effectiveness of the proposed control strategy under real-world scenarios, specifically in scenarios with low solar irradiance and varying module temperatures.

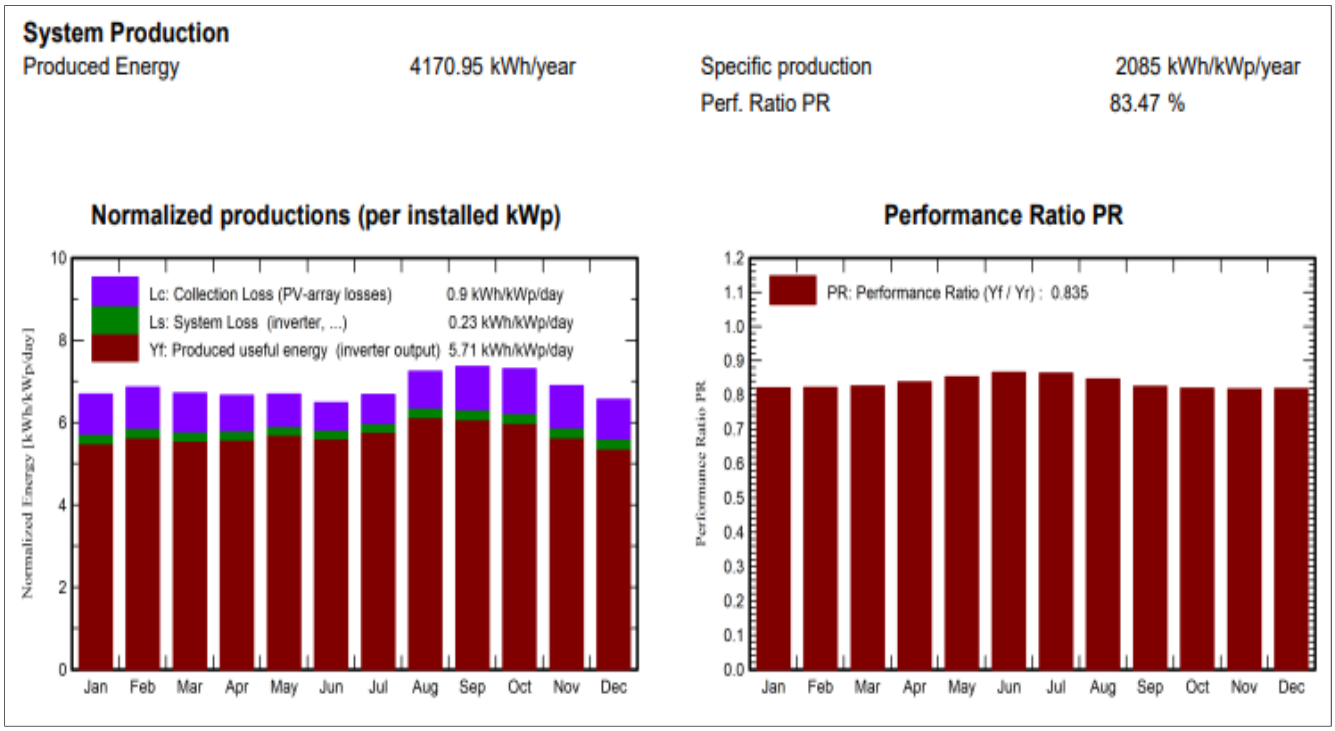

FIGURE 12. System performance ratio.

V. RESULTS AND DISCUSSION

In the system configuration, Case Study 1 aims to assess the energy infusion into the grid and potential energy dissipation by employing PVSyst software.

Moving on to Case Studies 2 through 4, the focus will shift towards scrutinizing the effectiveness of the suggested DDQN MPPT algorithm and ECG, with an emphasis on the EDSOGI-PLL Inverter control strategy, all of which will be implemented using MATLAB Simulink.

A. CASE STUDY 1 – FIXED TILT APPROACH

The evaluation of potential PV energy infusion into the grid and associated power losses was conducted using PVSyst simulation software. The study employed a fixed-tilt installation configuration with bifacial PV modules, utilizing meteorological data from Johannesburg, Alberton in the design. Figure 12 illustrates that 83.47% of the energy is generated at the inverter output, with corresponding annual energy losses of 16.53%. The energy available at the inverter output, contributing to the grid, amounted to 2085 kWh/kWp/year and 4171 kWh/year as shown in Table 4. These losses are attributed to various factors such as irradiance, module temperature, overload, and ohmic wiring loss within the PV array, as depicted in Figure 13. Additionally, inverter losses during operations also contribute to the overall energy loss. The findings suggest that the Johannesburg site is well-suited for solar renewable energies, yet there is room for improvement. The proposed DDQN MPPT controller with a centralized start up condition is expected to minimize energy losses caused by the PSC on the PV array side, while the inverter control technique ensures the injected power meets IEEE standards.

Therefore, Case Studies 2-4 will delve into the performance assessment of the proposed MPPT algorithm for accurately tracking the GMPP and reducing power losses at the PV array side, especially under challenging weather conditions. Furthermore, the ECG based on EDSOGI-PLL algorithm, is anticipated to enhance power quality in both steady-state and transient conditions.

The solar energy data for the given month shows a global horizontal irradiance of 2247.2 kWh/m^2, with a temperature of 17.56°C. The photovoltaic system's performance ratio (PR) is 0.835, resulting in an effective global efficiency (GlobEff) of 2448 kWh/m^2 and an annual energy production of 4339.3 kWh.

Table 5 offers a nuanced perspective on the environmental impact of the analyzed energy system, crucial for an energy and sustainability expert's comprehensive evaluation which were measured using PVSYST and HOMER software. The production of 2.61 metric tons of CO2, meticulously calculated from the underlying data, serves as a quantifiable measure of the direct emissions associated with the energy system. This figure underscores the imperative for cleaner and more sustainable energy sources, as reducing such emissions aligns with global efforts to mitigate climate change. Moreover, the replaced emissions total of 46.6 tCO2 highlights the transformative effect of the examined energy system.

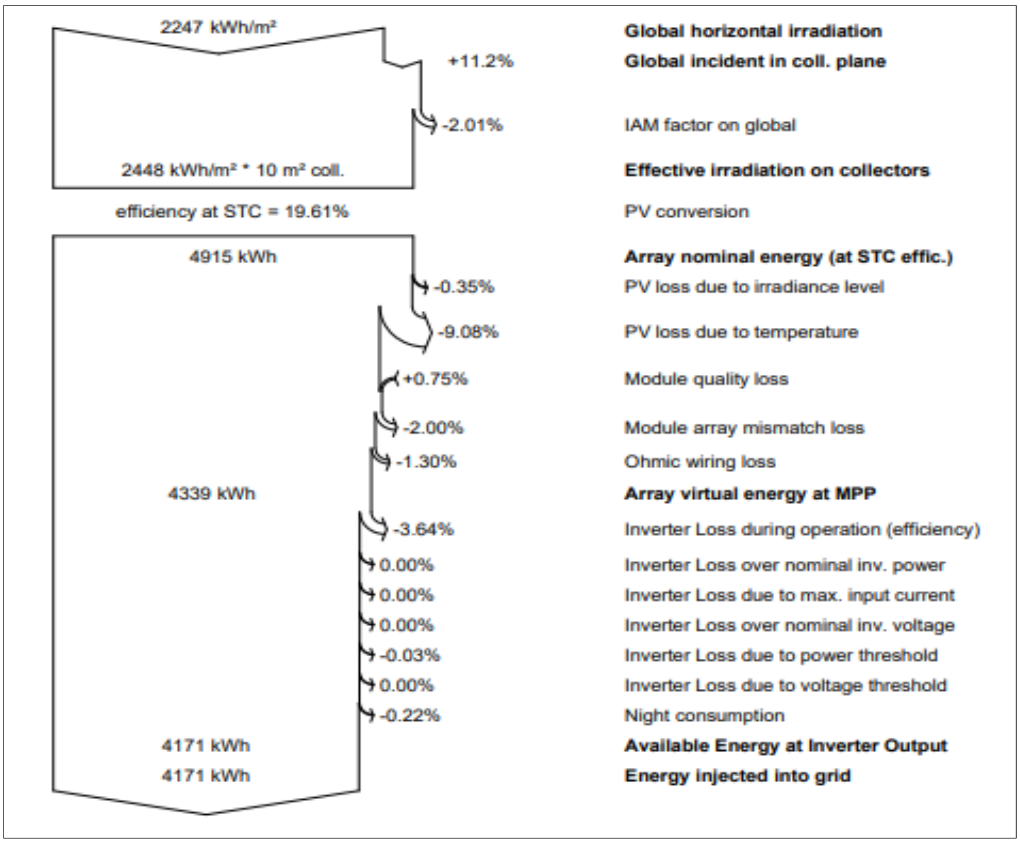

FIGURE 13. Loss diagram over the whole year.

TABLE 4. BPV Normalized performance.

Month	GlobHor kWh/m²	DiffHor kWh/m²	T_Amb °C	GlobInc kWh/m²	GlobEff kWh/m²	EArray kWh	PR ratio
January	235.8	70.3	21.18	207.4	201.7	355.4	0.821
February	198.8	63.46	21	192.1	187.5	329	0.822
March	191.1	58.36	20	208.3	204.1	358.6	0.827
April	161.3	42.62	17.12	199.9	196.8	348.5	0.838
May	144.3	31.23	14.53	207.2	204	366.9	0.866
June	126.0	23.75	11.57	194.4	191.8	349.4	0.863
July	139.1	24.61	11.36	207.2	204.5	371.2	0.847
August	167.8	28.29	14.76	224.5	221.6	394.2	0.826
September	192.2	41.87	18.14	220.9	217.3	379.1	0.82
October	224.2	53.01	20	226.8	221.2	386.4	0.82
November	230.1	61.99	20.09	206.7	200.7	352.6	0.818
December	236.6	76.10	21.2	203.3	196.9	347.9	0.819
Per Year	**2247.2**	**575.68**	**17.56**	**2498.5**	**2448**	**4339.3**	**0.835**

where:

GlobHor - Global horizontal irradiation.
DiffHor - Horizontal diffuse irradiation.
T_Amb - Ambient Temperature.
GlobInc - Global incident in coll. Plane.
GlobEff - Effective Global, corr. for IAM and shadings.
EArray - Effective energy at the output of the array.
E_Grid - Energy injected into grid.
PR - Performance Ratio.

By displacing conventional energy sources, it substantiates the tangible environmental benefits accrued through the adoption of renewable or cleaner technologies, further emphasizing the pivotal role such systems play in the transition toward a low-carbon future.

Delving deeper into the broader sustainability context, the calculated CO2 emission balance total of 37.8 tCO2 as shown

in figure 14 provides a net assessment, amalgamating both the produced and displaced emissions. This holistic perspective is essential for evaluating the overall environmental efficacy of the energy system. Additionally, considerations such as the system's 2085 kWh/kWp/year, its projected 30-year lifetime as depicted in Figure 14, and the annual degradation rate of 1.0% contribute to a comprehensive understanding of the system's long-term sustainability.

The incorporation of grid lifecycle emissions from the IEA list, specifically tailored to the South African context, further contextualizes the findings, illustrating the significance of accounting for regional variations in energy production.

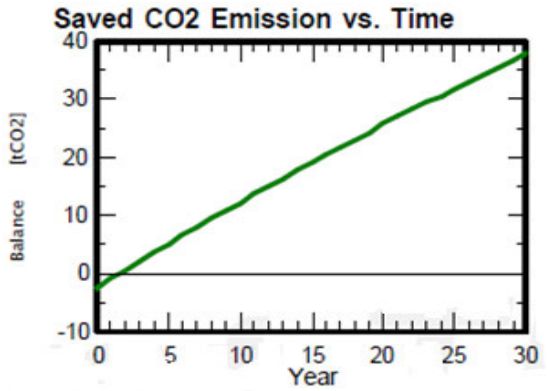

FIGURE 14. CO2 emission balance diagram.

1) RESOURCE CONSUMPTION IMPACT

The production and installation of PV modules and related components, which require substantial raw material consumption and energy-intensive manufacturing processes, may have major resource consumption consequences for the proposed integrated grid-tied PV system. Strategies like putting in place energy-efficient manufacturing procedures, creating strong material recycling programs, and carrying out thorough lifecycle assessments are crucial for minimizing these effects because they lower resource consumption and the environmental footprint of the system over its whole lifespan.

2) WASTE GENERATION IMPACT

If PV systems are decommissioned and broken or outdated components are disposed of improperly, trash—especially electronic waste, or e-waste—may be produced. Implementing end-of-life recycling programs, advocating extended producer responsibility legislation, and looking into potential reuse and repurposing for decommissioned components are just a few of the actions that must be taken to solve this problem in order to minimize landfill waste and maximize resource recovery. These tactics seek to minimize the environmental effects of waste creation and guarantee the responsible end-of-life management of PV systems.

TABLE 5. System life cycle emissions.

Parameters	Value
Produced Emissions	2.61 tCO2
Replaced Emissions	46.6 tCO2
Annual Degradation	1%
Lifetime	30 years
Grid Life Cycle Emissions	927 gCO2/kWh
CO2 Emission Balance	37.8 tCO2

TABLE 6. DDQN MPPT results.

Case Study	*Vmpp* (Vdc)	DC Link Voltage (V)	Tracking time (s)	PV efficiency (%)
2	28.9	289	0.012	99.23
3	28.77	287.7	0.013	98.57
4	28.65	286.5	0.014	98.04

TABLE 7. GEO MPPT results.

Case Study	*Vmpp* (Vdc)	DC Link Voltage (V)	Tracking time (s)	PV efficiency (%)
2	27.88	278.8	0.013	93.49
3	27.78	277.8	0.002	92.55
4	27.54	275.4	0.021	89.30

B. CASE STUDY 2 - DYNAMIC MPPT ALGORITHM PERFORMANCE UBDER PSC

The efficacy of the DDQN with EDSOGI-PLL based on HBM MPPT technique in optimizing PV power under PSC was verified and demonstrated. Figure 15 illustrates the successful tracking of the GMPP at 212.89 W per panel within a mere 0.012 seconds using the proposed DDQN approach. The results presented in Table 6 showcase a remarkable PV efficiency of 99.88%, with power losses limited to 0.12%. The proposed MPPT technique determined a PV current of 7.44A, *Vmpp* of 28.9Vdc and the combined DC link of 289Vdc. The duty ratio stabilized at $D = 0.55$ *at GMPP*. Notably, the input side of the inverter consistently received an optimal DC link voltage, courtesy of the proposed DDQN MPPT approach.

The DDQN algorithm was compared with the existing GEO MPPT algorithm as demonstrated in Figure 15. The GEO algorithm tracked the GMPP of 201W in 0.013 seconds. It recorded the PV efficiency of 93.49% as shown in Table 7. The GEO recorded Vmpp of 27.88Vdc and Impp of 7.21A respectively. The algorithm is inefficient as compared to the proposed DDQN.

The DDQN has benefits such as swift convergence, rapid settling, and minimal oscillation around the MPP resulting in high efficiency. In Case Study 2, the results

underscore the effectiveness of the DDQN MPPT technique in addressing PV power optimization challenges, attributed to its dynamic responsiveness, high tracking speed, convergence capabilities, and confidence-inspiring performance. The findings suggest that the proposed approach outperforms in handling dynamic scenarios and excels in ensuring efficient power extraction from the photovoltaic system under various conditions.

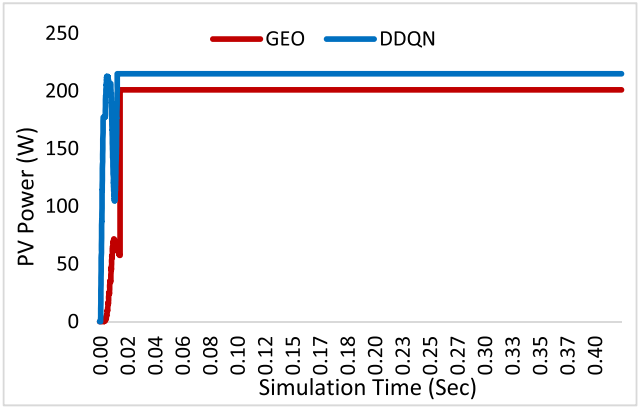

FIGURE 15. Case study 2 MPPT results with proposed DDQN with start-up condition.

The effectiveness of the ECG-EDSOGI-PLL based on HBM control strategy, was assessed under PSC and a linear load. In Figure 16, the percentage of current THD was depicted during a linear load. Typically, voltage harmonics stem from current harmonics induced by source impedance. Consequently, this paper focuses on measuring % THD_I. The proposed scheme exhibited a low THD of 0.26%, meeting the standards outlined by IEEE 519. Utilizing a substantial DC link inductor of 100mH resulted in minimal PV power ripple. The proposed scheme achieved a settling time of 0.14 seconds after tracking the GMPP. A system PF close to unity at 0.999 was recorded as shown in Table 8, aligning with the power quality analysis standards set by IEEE 1459.

TABLE 8. Inverter control strategies compared results.

ECG-EDSOGI-PLL inverter control algorithm			ASO Control strategy		
THDI (%)	System PF	Settling Time (s)	THDI (%)	System PF	Settling Time (s)
0.26%	0.999	0.13	2.52%	0.998	0.34
0.40%	0.999	0.27	5.57%	0.995	0.61
2.03%	0.998	0.30	12.83%	0.98	0.65

When examining the ASO control strategy in Figure 17 under linear load, the % current THD content was illustrated. The algorithm recorded a THD of 2.52%, slightly higher than the proposed method but still within the bounds of IEEE 519 standards. The ASO's settling time was 0.34 seconds after GMPP tracking, with a higher harmonics content compared to the proposed EM algorithm. The ASO exhibited a system PF of 0.998, marginally lower than the proposed scheme. The validation underscores that the proposed ECG, based on the EDSOGI-PLL inverter control algorithm, outperforms the ASO in terms of stability and power quality enhancement. This emphasizes the significance of deploying the proposed inverter control scheme to effectively mitigate harmonics and enhance power quality.

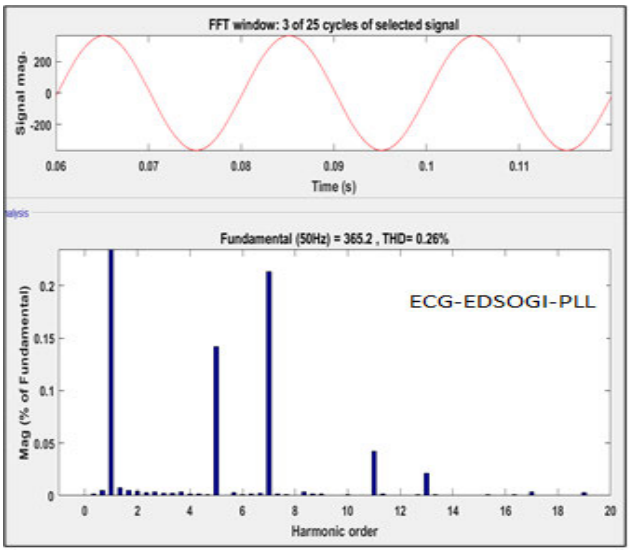

FIGURE 16. The THD performance results with ECG-EDSOGI-PLL with HBM (C2).

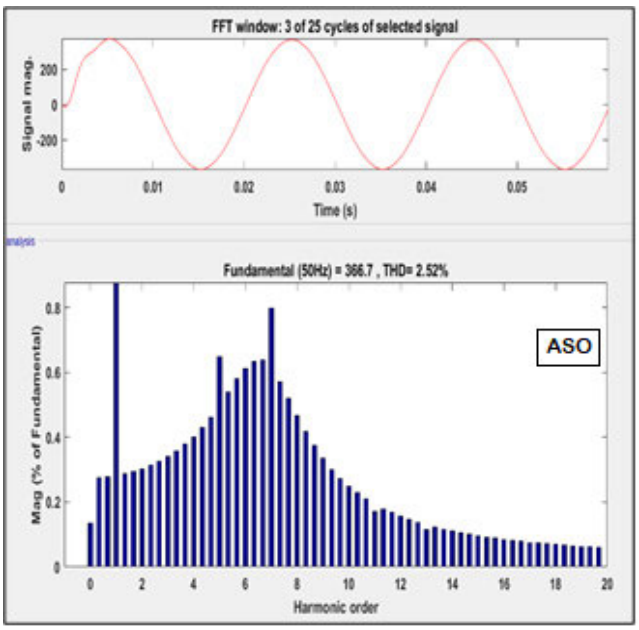

FIGURE 17. The THD performance results with ASO algorithm (C2).

C. CASE STUDY 3 - EXPLORING PATTERNED SOLAR IRRADIANCE VARIATION

In Case Study 3, alterations in weather conditions were introduced to evaluate the robustness of the recommended

DDQN MPPT approach in tracking the GMPP. The scenario also included the introduction of nonlinearity and a reduction in the DC link inductor. Figure 18 illustrates that the DDQN method adeptly tracked PV power at 210.11 W within a swift 0.013 seconds. Referencing Table 7, the PV efficiency stood at 98.57%, with energy losses limited to 1.43%. Employing the suggested MPPT technique yielded an optimal DC link *Vmpp* of 28.77V, PV current of 7.3A and DC link Voltage of 287.7V.

The GEO MPPT algorithm tracked GMPP of 199W in 0.02 seconds. The algorithm recorded PV voltage and current of 27.78Vdc and 7.16A respectively. The DC link voltage is 277.8Vdc and the efficiency of 92.56% as shown in Table 7. The algorithm demonstrated power losses of 7.44% under changing weather conditions. Analysis of Case Study 3 reveals that the DDQN MPPT algorithm's rapid-tracking capabilities enable it to sustain the desired inverter voltage even in challenging weather conditions as compared to GEO. The optimal duty ratio was established at $D = 0.57$. Notably, the proposed scheme demonstrated the ability to differentiate between the Local Maximum Power Point (LMPP) and the true GMPP. Leveraging restart conditions, the algorithm can identify shaded PV arrays and selectively perform GMPP tracking on those specific arrays, mitigating unnecessary power loss. The scheme exhibited swift convergence, minimal settling time, and reduced oscillations around the MPP. Simulation results indicate that the proposed DDQN MPPT technique is highly effective under PSC and excels in addressing PV power optimization challenges. Its dynamic and fast response, high tracking speed, convergence capabilities, and confidence ensure efficient performance. With lower energy losses and increased energy extraction from bifacial PV modules, the proposed approach contributes to a reduced energy payback time.

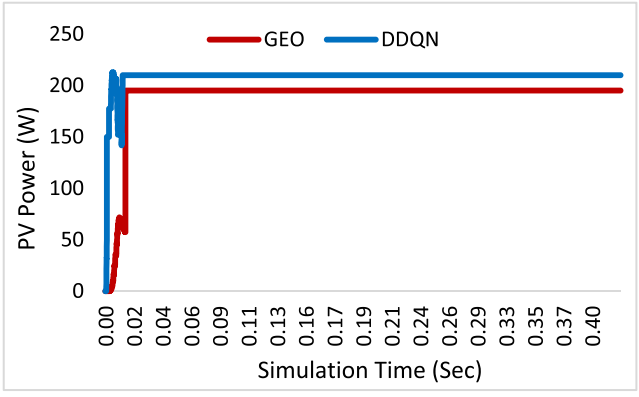

FIGURE 18. Case study 3 MPPT results with proposed DDQN with start-up condition.

Figure 19 showcases the percentage of current Total Harmonic Distortion (% current THD) content for the proposed ECG-EDSOGI-PLL inverter control strategy under varying loads and a reduced DC link inductor of 90mH. The proposed control scheme exhibited a commendable current THD of 0.40% during dynamic load changes, well within the stipulated limits of the IEEE 519 standard. Furthermore, the algorithm demonstrated an impressive system power factor of 0.999, aligning with the standards set by IEEE 1459. This indicates a phase alignment between current and voltage, minimizing power wastage. Figure 20 visually illustrates the proposed system generating a flawless sinusoidal current waveform, devoid of harmonic distortions.

However, a reduction in the DC link inductor resulted in an increased settling time of 0.27 seconds after tracking the Global Maximum Power Point (GMPP). Despite this, the THD content of the algorithm remained satisfactory when compared to the ASO scheme. The ECG-EDSOGI-PLL strategy's stability improvement in an AC system surpassed that of the ASO method. This enhancement may be attributed to the high-frequency voltage source controller switches employed during inverter operation; a feature not achievable in the ASO strategy.

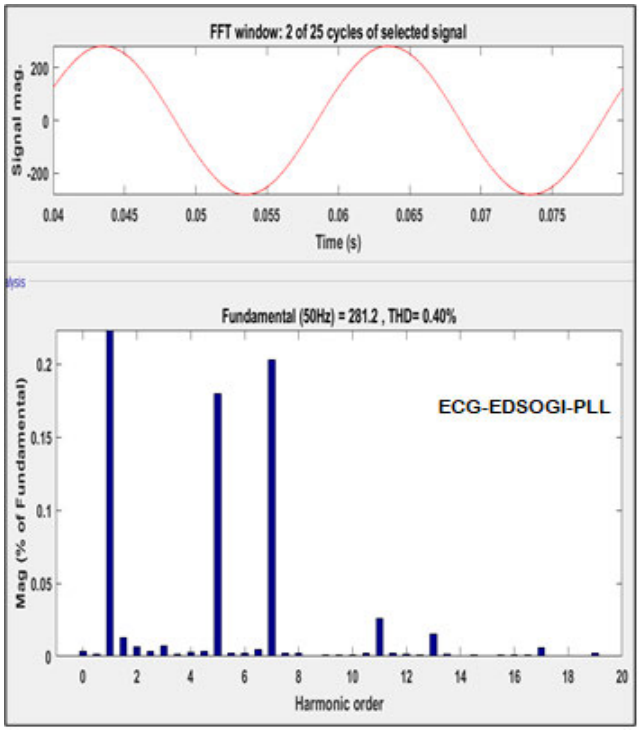

FIGURE 19. The THD performance results with ECG-EDSOGI-PLL with HBM (C3).

Figure 20 illustrates the % current THD content of the ASO during load variation and a reduced DC link inductor. The ASO algorithm recorded a high THD of 5.57%, surpassing the IEEE 519 standard limits under nonlinear load conditions. The settling time for the ASO was 0.61 seconds after tracking the GMPP, with significantly higher harmonics content compared to the proposed

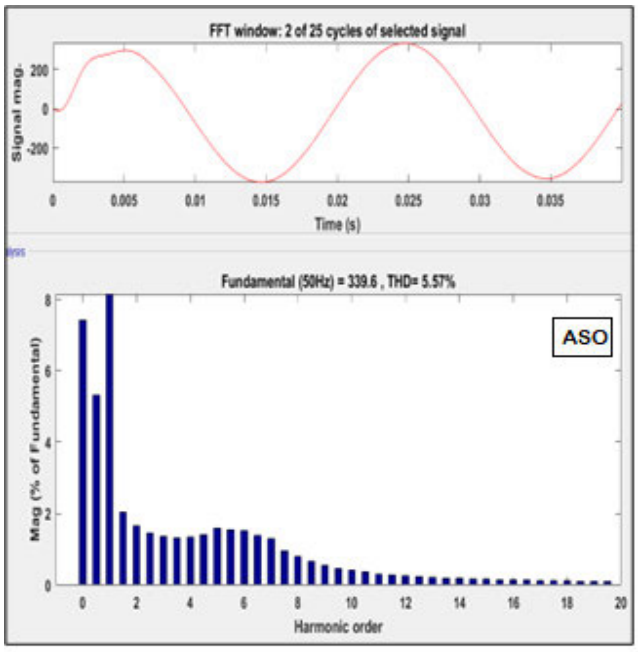

FIGURE 20. The THD performance results with ASO algorithm (C3).

ECG-EDSOGI-PLL control strategy. Despite a system power factor of 0.995, slightly lower than the proposed scheme, it is evident that the proposed ECG-EDSOGI-PLL algorithm outperforms in enhancing system performance, improving power controllability, and boosting stability margins.

D. CASE STUDY 4 - ENHANCING POWER QUALITY IN LOW IRRADIANCE ENVIRONMENTS

To assess the effectiveness of the proposed DDQN MPPT algorithm with a decentralized restart condition, alterations were made to the PSC by varying solar irradiance and module temperature. In this scenario, the proposed MPPT technique demonstrated its capability by successfully extracting the GMPP at 208.97 W, achieving a dynamic tracking speed of 0.014 seconds. The *Vmpp* recorded is 28.65 V and input side of the inverter produced a DC link voltage of 286.5 V, along with a recorded PV current of 7.3A.

Under the influence of the significant variability in weather conditions, characterized by the presence of multiple power peaks due to a large PSC, the proposed algorithm exhibited a PV efficiency of 98.04% and energy losses limited to 1.96%. Notably, the optimization of the PV system power was achieved at around $D = 0.64$. On the other hand, GEO MPPT algorithm achieved GMPP of 192W and PV efficiency of 89.30% respectively. The technique experienced a 10.7% decrease in power output due to dynamic PSC, indicating a failure to effectively track the GMPP amidst rapidly changing climatic conditions. The method recorded the Vmpp and Impp of 27.54Vdc and 6.97A distinctly.

Figure 21 illustrates the proposed DDQN's capability to discern the true GMPP instead of being confined to the LMPP. The proposed DDQN MPPT technique proved to be a significant contributor to power quality enhancement and the reduction of potential substantial energy losses under rapidly changing weather conditions. Moreover, the algorithm showcased robust performance in both the steady-state and transient states of the system, reinforcing its effectiveness across diverse operational scenarios. This substantiates the claim that the proposed DDQN MPPT technique holds promise for substantial improvements in power quality and efficiency, particularly in the face of dynamically changing environmental conditions.

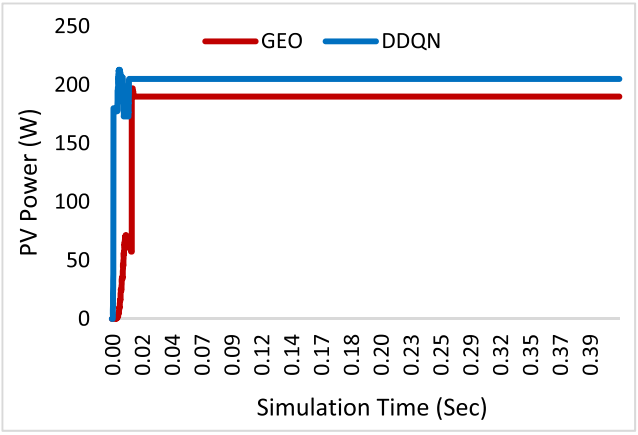

FIGURE 21. Case study 4 MPPT results with proposed DDQN with start-up condition.

In Figure 22, the percentage current THD for the proposed ECG-EDSOGI-PLL during nonlinear loads and a reduced DC link inductor of 70mH is depicted. The proposed strategy achieved a THD of 2.03% under dynamic load changes, meeting the criteria set by the IEEE 519 standard. The algorithm exhibited an impressive system power factor of 0.998, well within the bounds of the IEEE 1459 standard. However, a reduction in the DC link inductor resulted in an increased settling time of 0.30 seconds after tracking the GMPP. Despite this, the THD content of the algorithm remained satisfactory compared to the ASO strategy. The proposed system not only enhances the stability of the utility grid but also minimizes harmonics content, providing improved controllability and stability for both active and reactive power in the grid, as outlined in Appendix A.

Figure 23 illustrates the grid current %THD level of the ASO during load variations and a reduced DC link inductor. The ASO algorithm recorded a high THD of 12.83%, surpassing the limits of the IEEE 519 standard. The increased THD in Figure 23 is primarily due to the ASO Algorithm, which does not effectively regulate or control the grid current under load variations and with a reduced DC link

inductor. The settling time for the ASO was 0.65 seconds after tracking the GMPP, accompanied by higher harmonics content compared to the proposed inverter control strategy, as detailed in Appendix B.

The QRNN recorded the THD of 2.34%, which is also higher than of the proposed ECG-EDSOGI-PLL as shown in Figure 24 and Appendix C. However, QRNN performed better than ASO which demonstrated the highest THD level. The ASO method also exhibited phase imbalance due to the low DC link inductor and nonlinear load. With a system power factor of 0.98, slightly lower than that of the proposed scheme, it is evident that the proposed inverter control strategy significantly outperforms the ASO in terms of stability and improved power quality.

The results underscore the effectiveness of the proposed ECG-EDSOGI-PLL strategy in ensuring grid stability, harmonics mitigation, and enhanced control overactive and reactive power, providing valuable insights for applications in diverse scenarios as compared to the ASO and QRNN control strategies.

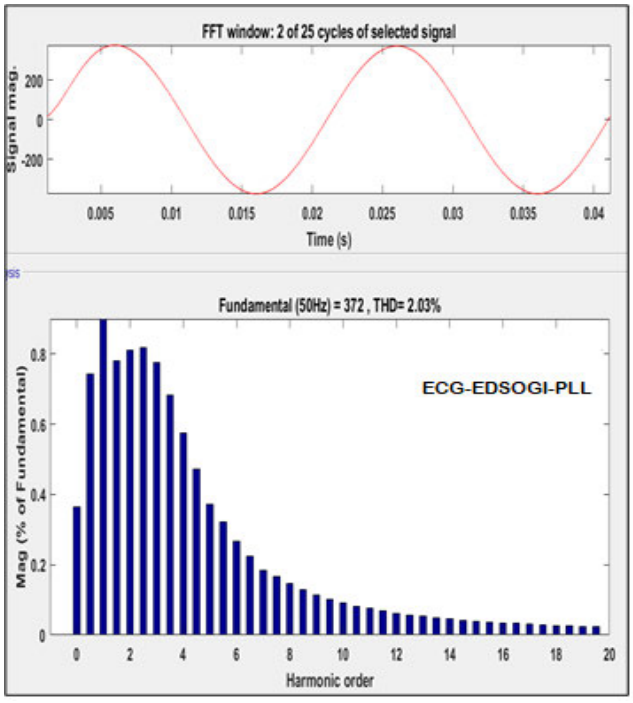

FIGURE 22. The THD performance results with ECG-EDSOGI-PLL with HBM (C4).

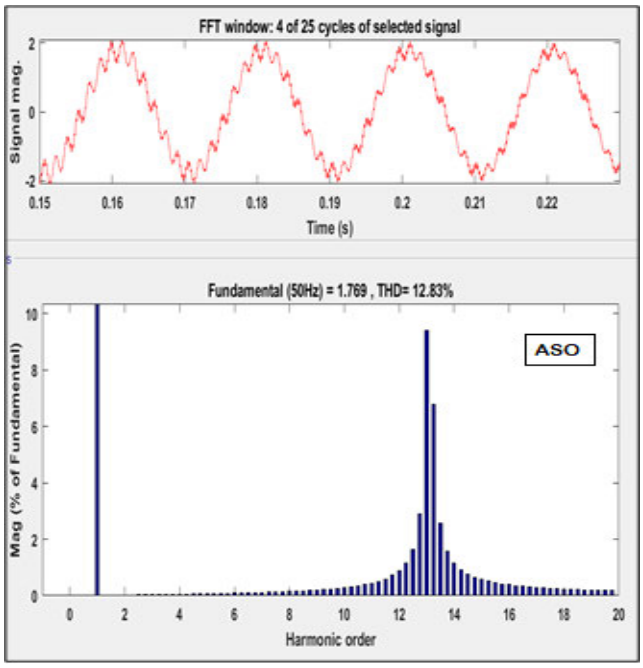

FIGURE 23. The THD performance results with ASO algorithm (C4).

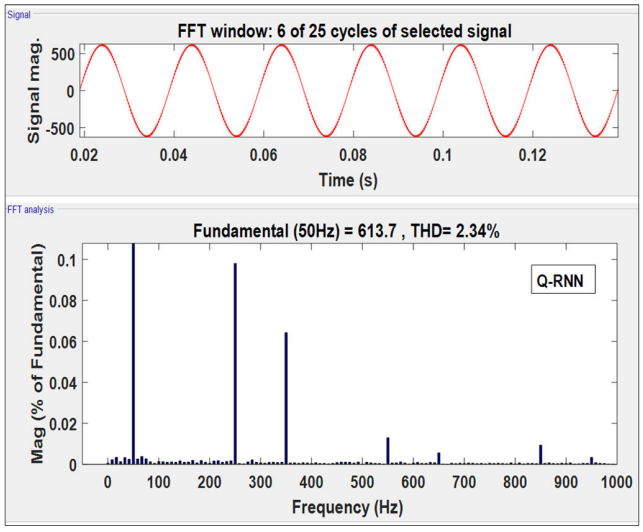

FIGURE 24. The THD performance results with QRNN algorithm (C4).

E. SUMMARY

The comparative evaluation of the proposed ECG-EDSOGI-PLL inverter control algorithm with the recent ASO and QRNN from the literature is conducted using the parameters of contemporary bifacial PV panel technology integrated into the Simulink file, resulting in satisfactory simulation outcomes. Table 9 is employed to delineate the distinctions between the three control strategies across various characteristics. The findings unequivocally demonstrate the superiority of the proposed ECG-EDSOGI-PLL scheme over the ASO and QRNN, particularly in its adherence to IEEE 519 standard limits under both linear and nonlinear load conditions. The proposed method boasts several advantages, including high performance, cost-effectiveness, ease of compensatory tuning, double-loop harmonic mitigation, remarkable accuracy, reduced settling time, and a shorter energy payback time.

However, caution is advised in selecting the DC link inductor value, particularly at very low modulation indices. The ASO, on the other hand, faces challenges in reducing

TABLE 9. Inverter control strategies compared results.

Characteristics	ASO	QRNN	ECG-EDSOGI-PLL
Type of filter	Adaptive	Adaptive	Adaptive
Oscillations	High	Medium	less
Complexity	Medium	Medium	Medium
Amplitude tracking	Good	Good	Excellent
Grid Synchronization	Slow	Fast	Rapid
Accuracy	Moderate	Moderate	Good
Frequency tracking	Good	Good	Better
Settling time	Slow	Medium	Rapid
THD under linear load	Good	Good	Excellent
THD under nonlinear load	Exceeds IEEE 519 limits	Compliance to IEEE 519	Compliance to IEEE 519
Payback time	More	Less	Less
Power quality	Poor	Good	Good

THD levels and exceeds IEEE 519 standards under transient states. While the ASO exhibits benefits such as moderate complexity and good amplitude tracking, it is burdened with drawbacks such as heightened harmonics and oscillations, voltage spikes, imbalance, and a prolonged settling time. The QRNN control strategy performed better as compared to ASO, demonstrating moderate accuracy, fast grid synchronization and good power quality. These comparative results underscore the overall superior performance of the proposed ECG-EDSOGI-PLL inverter control algorithm, offering a compelling solution for applications where precision, stability, and compliance with power quality standards are imperative considerations.

VI. CONCLUSION

The paper introduces a comprehensive and innovative approach for managing grid-connected fixed tilt bifacial PV systems. The proposed ECG algorithm, coupled with an EDSOGI-PLL based on HBM and a DDQN maximum power point tracking algorithm, exhibits superior performance in addressing critical challenges faced by PV systems. The DDQN MPPT algorithm, with its centralized start-up condition computation, ensures stable DC voltage levels and minimizes fluctuations during transient states, significantly enhancing energy efficiency under PSC. Moreover, the ECG-EDSOGI-PLL inverter control strategy, integrated with a Sequential Cascaded HBM, successfully mitigates harmonics, attains grid synchronization, and estimates symmetrical components under unbalanced grid conditions, showcasing its adaptability and effectiveness.

The presented case studies validate the robustness and efficacy of the proposed strategies. Through simulations and analyses, the DDQN MPPT algorithm consistently achieves swift and accurate tracking of the GMPP under various conditions, reducing energy losses and improving power quality as compared to GEO MPPT algorithm.

The ECG-EDSOGI-PLL control strategy outperforms the conventional ASO method, demonstrating enhanced stability, lower THD, and adherence to IEEE standards. The thorough examination of the proposed system's environmental impact reveals a significant reduction in CO2 emissions and attests to the system's potential for sustainable energy production. Overall, this research contributes valuable insights and practical solutions to the field of grid-connected bifacial PV systems, emphasizing the proposed algorithms' prowess in addressing challenges and optimizing the performance of renewable energy systems.

In brief, the principal result of this research can be summarized as follows:

- The energy contribution to the grid from the inverter output amounted to 2085 kWh/kWp/year and 4171 kWh/year.
- The DDQN algorithm achieved an average PV efficiency of 98% under dynamic PSC, establishing it as a dependable and effective solution for maintaining high efficiency in fluctuating environmental conditions.
- Simulation results of ECG-EDSOGI-PLL confirm adherence to IEEE 519 Standards, with THD below 3% and power factor approximately equal to 1.
- Additionally, the meticulous calculation of 2.61 metric tons of CO2 production serves as a quantifiable measure of the direct emissions associated with the energy system, highlighting its environmental impact.

Exploring a diverse range of research avenues remains essential, given the limitations inherent in any single study, as is common in most research endeavors. Subsequent investigations could shift their emphasis towards alternative machine learning methodologies, encompassing techniques like dimensionality reduction (DR), generalized discriminant analysis (GDA), and principal component analysis (PCA).

APPENDIX A
3 PHASE GRID VOLTAGES AND CURRENTS AFTER ECG-EDSOGI-PLL COMPENSATOR

See Fig. 25.

APPENDIX B
3 PHASE GRID VOLTAGES AND CURRENTS AFTER ASO COMPENSATOR

See Fig. 26.

APPENDIX C
3 PHASE GRID VOLTAGES AND CURRENTS AFTER Q-RNN COMPENSATOR

See Fig. 27.

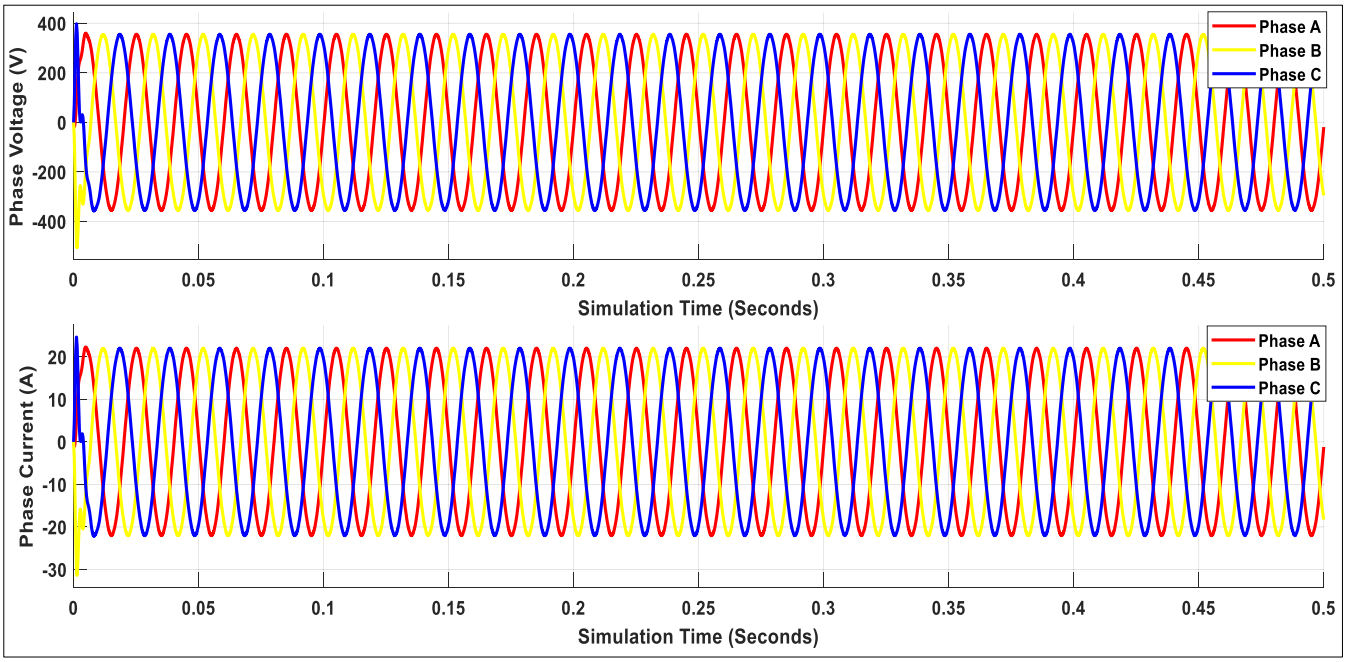

FIGURE 25. 3 Phase Voltage and current with ECG-EDSOGI-PLL.

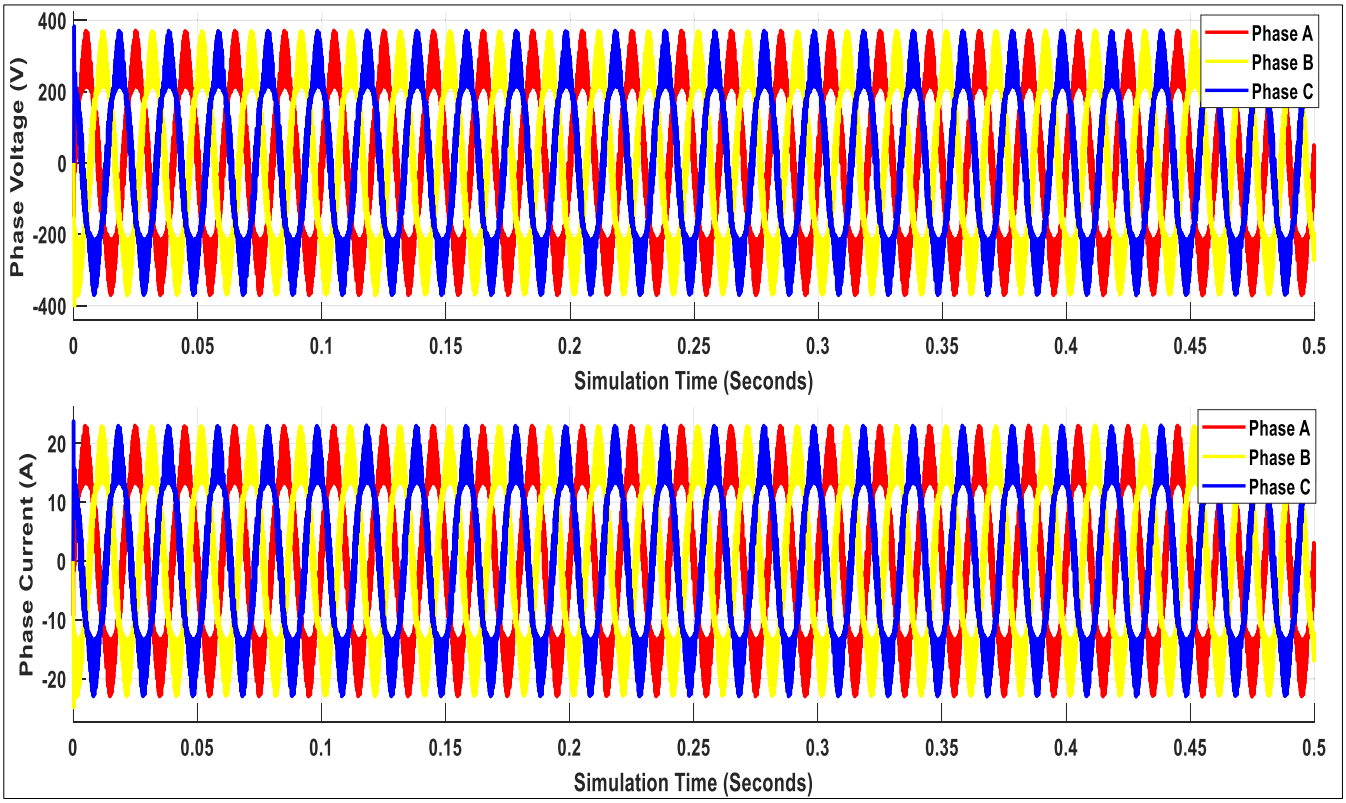

FIGURE 26. 3 Phase Voltage and current without control strategy.

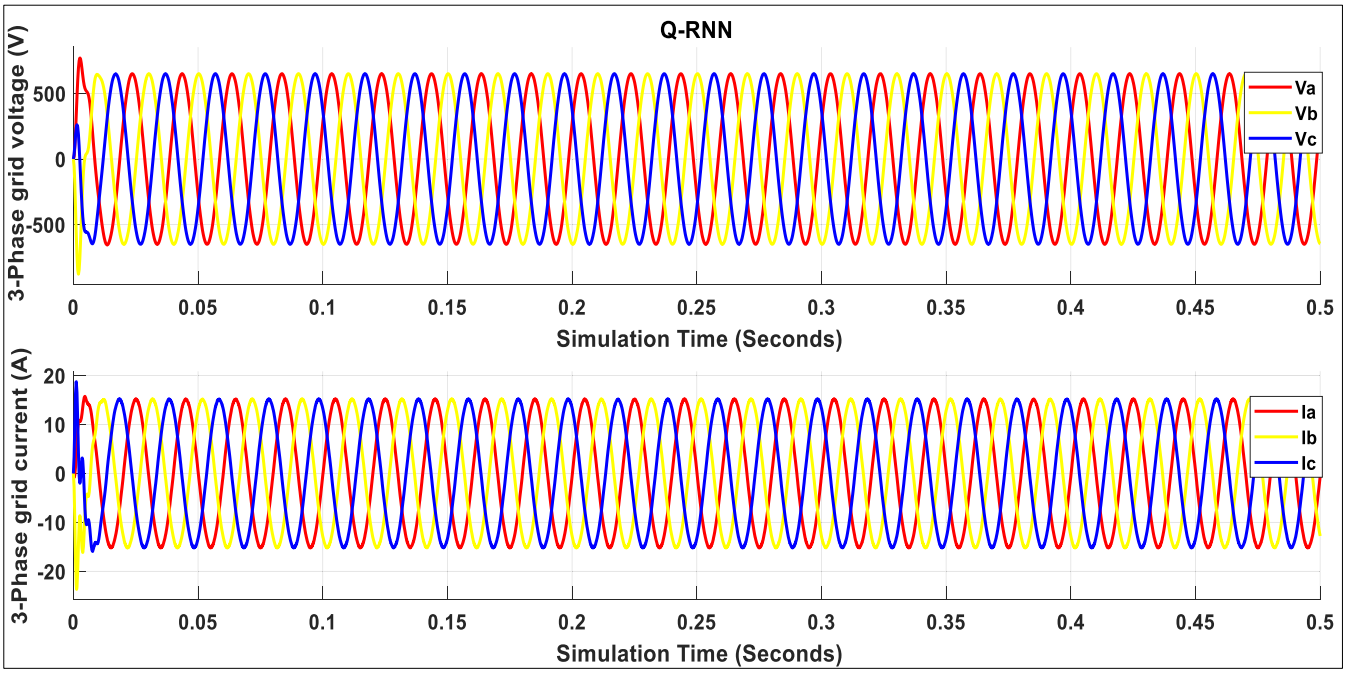

FIGURE 27. 3 Phase Voltage and current with Q-RNN.

REFERENCES

[1] M. S. Nkambule, A. N. Hasan, and A. Ali, "MPPT under partial shading conditions based on perturb & observe and incremental conductance," in *Proc. 11th Int. Conf. Electr. Electron. Eng. (ELECO)*, Nov. 2019, pp. 85–90.

[2] S. Bhaduri and A. Kottantharayil, "Mitigation of soiling by vertical mounting of bifacial modules," *IEEE J. Photovolt.*, vol. 9, no. 1, pp. 240–244, Jan. 2019.

[3] U. K. Kalla and M. Mantri, "An adaptive control of voltage source converter based scheme for grid connected solar PV–battery system," in *Proc. IEEE 7th Power India Int. Conf. (PIICON)*, Nov. 2016, pp. 1–5.

[4] D. Pilakkat and S. Kanthalakshmi, "An improved P&O algorithm integrated with artificial bee colony for photovoltaic systems under partial shading conditions," *Sol. Energy*, vol. 178, pp. 37–47, Jan. 2019.

[5] A. Ramyar, H. Iman-Eini, and S. Farhangi, "Global maximum power point tracking method for photovoltaic arrays under partial shading conditions," *IEEE Trans. Ind. Electron.*, vol. 64, no. 4, pp. 2855–2864, Apr. 2017.

[6] X. Tao, J. Xin, S. Zhang, Z. Xu, Z. Ye, K. Wang, B. Chen, and N. Zhou, "A novel Harris-hawk-optimization-based maximum-power-point-tracking control strategy for a grid-connected PV power-generation system," *Energies*, vol. 17, no. 1, p. 76, Dec. 2023, doi: 10.3390/en17010076.

[7] Z.-K. Fan, K.-L. Lian, and J.-F. Lin, "A new golden eagle optimization with stooping behaviour for photovoltaic maximum power tracking under partial shading," *Energies*, vol. 16, no. 15, p. 5712, Jul. 2023, doi: 10.3390/en16155712.

[8] K.-H. Huang, K.-H. Chao, Y.-P. Kuo, and H.-H. Chen, "Maximum power point tracking of photovoltaic module arrays based on a modified gray wolf optimization algorithm," *Energies*, vol. 16, no. 11, p. 4329, May 2023, doi: 10.3390/en16114329.

[9] A. M. Eltamaly, M. S. Al-Saud, A. G. Abokhalil, and H. M. Farh, "Photovoltaic maximum power point tracking under dynamic partial shading changes by novel adaptive particle swarm optimization strategy," *Trans. Inst. Meas. Control*, vol. 42, no. 1, pp. 104–115, Jan. 2020.

[10] E. Halassa, L. Mazouz, A. Seghiour, A. Chouder, and S. Silvestre, "Revolutionizing photovoltaic systems: An innovative approach to maximum power point tracking using enhanced dandelion optimizer in partial shading conditions," *Energies*, vol. 16, no. 9, p. 3617, Apr. 2023, doi: 10.3390/en16093617.

[11] A. M. Eltamaly, M. S. Al-Saud, and A. G. Abokhalil, "A novel scanning bat algorithm strategy for maximum power point tracker of partially shaded photovoltaic energy systems," *Ain Shams Eng. J.*, vol. 11, no. 4, pp. 1093–1103, Dec. 2020.

[12] K. K. Mohammed, S. Buyamin, I. Shams, and S. Mekhilef, "Maximum power point tracking based on adaptive neuro-fuzzy inference systems for a photovoltaic system with fast varying load conditions," *Int. Trans. Electr. Energy Syst.*, vol. 31, May 2021, Art. no. e12904.

[13] J.-Y. Shi, F. Xue, Z.-J. Qin, W. Zhang, L.-T. Ling, and T. Yang, "Improved global maximum power point tracking for photovoltaic system via cuckoo search under partial shaded conditions," *J. Power Electron.*, vol. 16, no. 1, pp. 287–296, Jan. 2016.

[14] L. Wu, X. Zhang, Q. Liu, and C. Fan, "MPPT control algorithm for photovoltaic power generation based on multi-universe optimization algorithm," *J. Sol. Energy*, vol. 44, pp. 204–211, Jun. 2023.

[15] C. Ling, W. Honghua, and H. Wei, "Simulation study of photovoltaic power generation in maximum power point tracking based on CSA-FPI algorithm," *Electr. Meas. Instrum.*, vol. 8, pp. 39–44, Jul. 2015.

[16] R. Wang, H. Gao, and X. Zhang, "Photovoltaic MPPT algorithm based on GA-GRU neural network," *J. Sol. Energy*, vol. 44, pp. 212–219, Sep. 2023.

[17] S. Padmanaban, C. Dhanamjayulu, and B. Khan, "Artificial neural network and Newton Raphson (ANN-NR) algorithm based selective harmonic elimination in cascaded multilevel inverter for PV applications," *IEEE Access*, vol. 9, pp. 75058–75070, 2021.

[18] R. B. Peesapati and G. Panda, "An optimal current control scheme in grid-tied hybrid energy system with active power filter for harmonic mitigation," *Int. Trans. Electr. Energy Syst.*, vol. 30, no. 3, Mar. 2020, Art. no. e12183.

[19] Q. Liu, Y. Li, L. Luo, Y. Peng, and Y. Cao, "Power quality management of PV power plant with transformer integrated filtering method," *IEEE Trans. Power Del.*, vol. 34, no. 3, pp. 941–949, Jun. 2019.

[20] M. Ghiasi, "Technical and economic evaluation of power quality performance using FACTS devices considering renewable generations," *Renew. Energy Focus*, vol. 29, pp. 49–62, Jun. 2019.

[21] M. S. Nkambule, "Improving power quality for a grid connected photovoltaic system using artificial intelligence techniques," Ph.D. thesis, Dept. Elect. Electron. Eng., Univ. Johannesburg, Johannesburg, South Africa, 2023. [Online]. Available: https://hdl.handle.net/10210/505365

[22] M. Fallah, M. Imani, H. M. Kojabadi, M. Abarzadeh, M. T. Bina, and L. Chang, "Novel structure for unbalance, reactive power and harmonic compensation based on VFF-RLS and SOGI-FLL in three phase four wire power system," in *Proc. IEEE Energy Convers. Congr. Expo. (ECCE)*, Sep. 2015, pp. 6254–6260.

[23] B. Singh, C. Jain, and S. Goel, "ILST control algorithm of single-stage dual purpose grid connected solar PV system," *IEEE Trans. Power Electron.*, vol. 29, no. 10, pp. 5347–5357, Oct. 2014.

[24] S. Pradhan, I. Hussain, B. Singh, and B. K. Panigrahi, "Modified VSS-LMS-based adaptive control for improving the performance of a single-stage PV-integrated grid system," *IET Sci., Meas. Technol.*, vol. 11, no. 4, pp. 388–399, Jul. 2017.
[25] R. K. Agarwal, I. Hussain, and B. Singh, "LMF-based control algorithm for single stage three-phase grid integrated solar PV system," *IEEE Trans. Sustain. Energy*, vol. 7, no. 4, pp. 1379–1387, Oct. 2016.
[26] P. N. Babu, R. Peesapati, and G. Panda, "An adaptive differentiation frequency based advanced reference current generator in grid-tied PV applications," *IEEE J. Emerg. Sel. Topics Power Electron.*, vol. 8, no. 4, pp. 3502–3515, Dec. 2020.
[27] X. Guo, W. Wu, and Z. Chen, "Multiple-complex coefficient-filter-based phase-locked loop and synchronization technique for three-phase grid-interfaced converters in distributed utility networks," *IEEE Trans. Ind. Electron.*, vol. 58, no. 4, pp. 1194–1204, Apr. 2011.
[28] R. Hosseini and S. Sra, "An alternative to EM for Gaussian mixture models: Batch and stochastic Riemannian optimization," *Math. Program.*, vol. 181, no. 1, pp. 187–223, May 2020.
[29] J. Li-Jun, J. Miao-Miao, Y. Guang-Yao, C. Yi-Fan, L. Rong-Zheng, Z. Hai-Peng, and Z. Ke, "Unbalanced control of grid-side converter based on DSOGI-PLL," in *Proc. IEEE 10th Conf. Ind. Electron. Appl. (ICIEA)*, Auckland, New Zealand, Jun. 2015, pp. 1145–1149.
[30] M. Nkambule, A. Hasan, A. Ali, and T. Shongwe, "A novel control strategy in grid-integrated photovoltaic system for power quality enhancement," *Energies*, vol. 15, no. 15, p. 5645, Aug. 2022, doi: 10.3390/en15155645.
[31] NASA. (Feb. 2, 2022). *Power Single Point*. [Online]. Available: https://power.larc.nasa.gov/data-access-viewer
[32] Global Solar Atlas. (2023). *Photovoltaic Power Potential*. Accessed: Oct. 3, 2023. [Online]. Available: https://www.worldweatheronline.com/limpopo-weather-averages/gauteng/za.aspx
[33] S. J. Alam and S. R. Arya, "Control of UPQC based on steady state linear Kalman filter for compensation of power quality problems," *Chin. J. Electr. Eng.*, vol. 6, no. 2, pp. 52–65, Jun. 2020.
[34] M. S. Nkambule, A. N. Hasan, and T. Shongwe, "Performance and techno-economic analysis of optimal hybrid renewable energy systems for the mining industry in South Africa," *Sustainability*, vol. 15, no. 24, p. 16766, Dec. 2023, doi: 10.3390/su152416766.

MPHO SAM NKAMBULE received the bachelor's, M.Phil., and Ph.D. degrees in electrical and electronics engineering from the University of Johannesburg, Johannesburg, South Africa, in 2017, 2020, and 2023, respectively. He is currently a Postdoctoral Research with the University of Johannesburg. His research interests include solar photovoltaic systems, wind energy, battery energy storage, power electronics, power quality, artificial intelligence, and MPPT controller designs for energy harvesting systems.

ALI NABIL HASAN received the B.Eng. degree in electrical and electronic engineering from The Hashemite University, Jordan, in 2005, the M.Eng. degree in electrical engineering from Northwest University, South Africa, in 2010, and the D.Ing. (Ph.D.) degree in electrical and electronic engineering from the University of Johannesburg, South Africa, in 2014. He was a Senior Lecturer with the Electrical Engineering Technology Department, University of Johannesburg, South Africa. He is currently a Professor with the Higher Colleges of Technology, Abu Dhabi. His research work focuses on the applications of artificial intelligence in energy, power, and communication systems.

THOKOZANI SHONGWE (Senior Member, IEEE) received the B.Eng. degree in electronic engineering from the University of Swaziland, Swaziland, in 2004, the M.Eng. degree in telecommunications engineering from the University of the Witwatersrand, South Africa, in 2006, and the D.Eng. degree from the University of Johannesburg, South Africa, in 2014. He is currently an Associate Professor with the Department of Electrical and Electronic Engineering Technology, University of Johannesburg. His research interests include digital communications and error-correcting coding, power-line communications, cognitive radio, smart grids, visible light communications, machine learning, and artificial intelligence. He was a recipient of the 2014 University of Johannesburg Global Excellence Stature (GES) Award, which was awarded to him to carry out his postdoctoral research with the University of Johannesburg. In 2016, he was a recipient of the TWAS-DFG Cooperation Visits Programme funding to do research in Germany. Other awards that he has received in the past are the Postgraduate Merit Award Scholarship to pursue his master's degree from the University of the Witwatersrand, in 2005, which is awarded on a merit basis. In 2012, he (and his coauthors) received an award for the Best Student Paper from the IEEE ISPLC 2012 (Power Line Communications Conference), Beijing, China.